# Impact of heat loss from storage tank with phase change material on the performance of a solar-assisted heat pump system

Yantong Li[a], Natasa Nord[b], Huibin Yin[a,*], Gechuanqi Pan [a,*]

[a]Guangdong Provincial Key Laboratory of Multi-energy Complementary Distributed Energy Systems, Dongguan University of Technology, Dongguan 523808, China

[b]Department of Energy and Process Engineering, Norwegian University of Science and Technology, Trondheim NO-7491, Norway

[*]E-mail address: yinhb@dgut.edu.cn; phone: (+86) 0769-22861808,
2022003@dgut.edu.cn; phone: (+86) 0769-22862039

## Abstract

Solar-assisted heat pump systems can address the drawbacks of traditional heat pumps, which have high operating costs, and solar collectors, which cannot provide continuous heat throughout the day. A storage tank is a common device in solar-assisted heat pumps. However, the impact of heat loss from a storage tank with phase change material on the performance of solar-assisted heat pump system is still unknown. Therefore, this study investigated the impact of heat loss from a storage tank with phase change material on the energy, economic, environmental, and technical performance of a solar-assisted heat pump system. A case study for swimming pool application was conducted. The simulation platform was built using TRNSYS and MATLAB. Performance comparison between systems with and without heat loss from a storage tank with phase change material was conducted. Results indicated that when the heat loss coefficient varied from 2 W/($m^2$ • K) to 12 W/($m^2$ • K), total electricity use, operating cost, thermal uncomfortable ratio, and $CO_2$ emission increased by up to 22.3%, 16.8%, 242.9%, and 22.3%, respectively. This study helped scholars understand the importance of considering heat loss from storage tanks with phase change material in assessing the performance of solar-assisted heat pump systems.

**Keywords:** Latent heat; Energy storage; Solar Energy; Air source

## Graphical Abstract

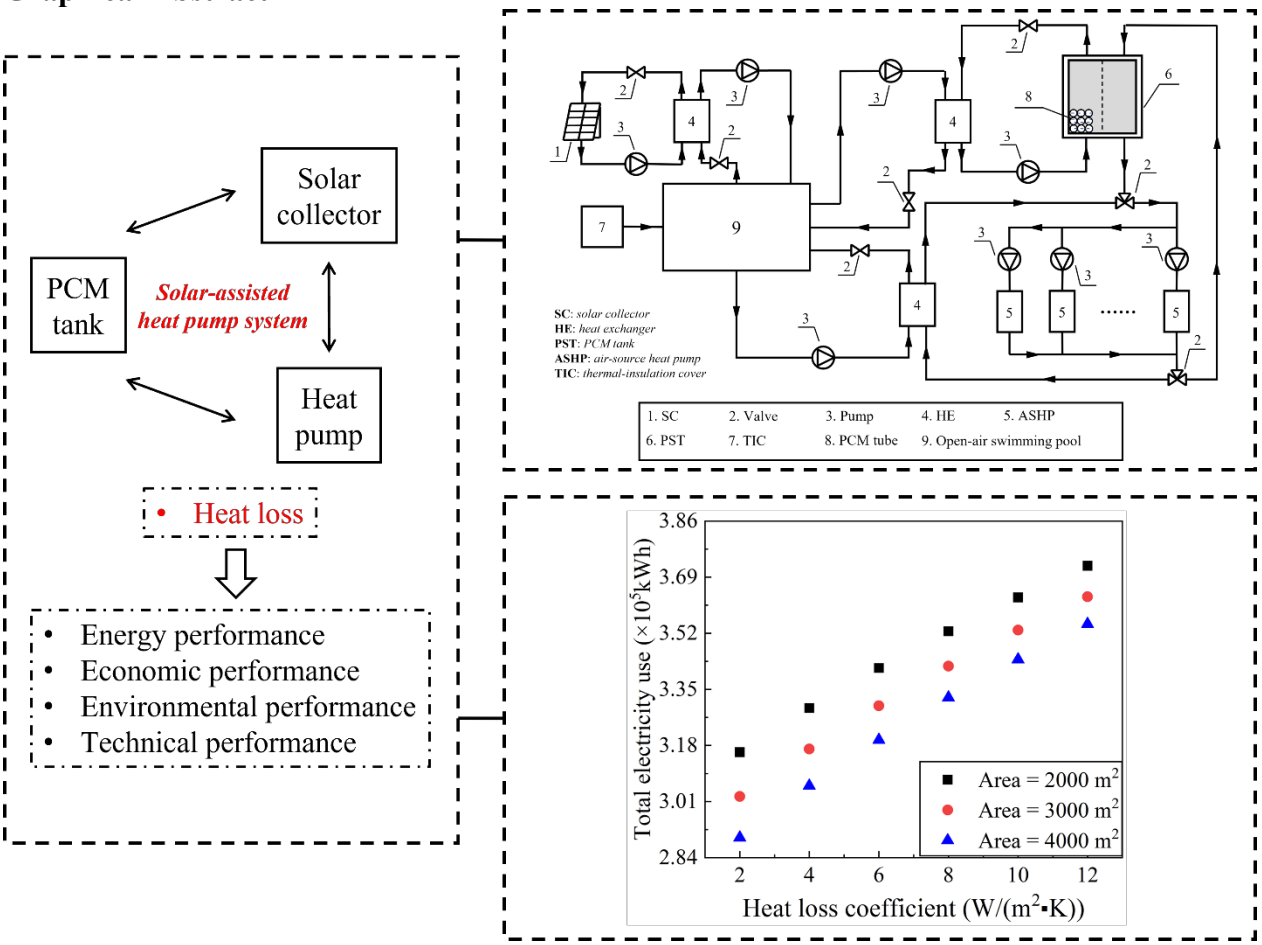

**Nomenclature**

| | |
|---|---|
| $A$ | Surface area ($m^2$) |
| $b$ | Weight factor (-) |
| $c$ | Specific heat (kJ/(kg·K)) |
| $ce$ | Electricity cost (€) |
| $cn$ | $CO_2$ emission (ton) |
| $ct$ | Capital cost (€) |
| $es$ | Electricity use (kWh) |
| $H$ | Enthalpy (kJ/kg) |
| $h$ | Coefficient (W/($m^2$·K))) |
| $hv$ | Volumetric heat transfer coefficient (W/($m^3$·K)) |
| $k$ | Thermal conductivity (W/(m·K)) |
| $ot$ | Operating cost (€) |
| $oy$ | Emission coefficient (ton/kWh) |
| $q$ | Heat flux (W) |
| $S$ | Score (-) |
| $T$ | Temperature (°C) |
| $t$ | Moment (h) |
| $tur$ | Thermal uncomfortable ratio (-) |
| $U$ | Response parameter |
| $um$ | A variable (-) |
| $V$ | Volume ($m^3$) |
| $v$ | Velocity (m/s) |
| $x$ | Distance (m) |

*Abbreviations*

| | |
|---|---|
| ASHP | Air-source heat pump |
| COP | Coefficient of performance (-) |
| $CO_2$ | Carbon dioxide |
| HE | Heat exchanger |
| SC | Solar collector |
| TIC | Thermal-insulation cover |

*Subscripts*

| | |
|---|---|
| $a$ | ASHP |
| $cd$ | Conduction |
| $co$ | Convection |
| $cx$ | Coded |
| $dm$ | Demand |
| $ec$ | Energy |
| $er$ | Evaporation |
| $fk$ | Off-peak period |
| $hl$ | Heat loss |
| $mn$ | Minimum |
| $mx$ | Maximum |
| $o$ | Overall performance |
| $ok$ | On-peak period |
| $p$ | Pump |
| $pw$ | Pool water |
| $ra$ | Radiation |
| $rs$ | Refilling fresh water |
| $s$ | Setting |
| $so$ | Solar |
| $t$ | Total |
| $tl$ | Total open |
| $wp$ | Water in PST |

Greeks

| | |
|---|---|
| $\epsilon$ | Water fraction (-) |
| $\rho$ | Density (kg/$m^3$) |

| | | | |
|---|---|---|---|
| PCM | Phase change material | $\tau$ | Time (s) |
| PST | PCM tank | | |

1

## 1. Introduction

Due to the carbon neutrality goals set by many countries, a wide range of renewable energy technologies, including photovoltaic plant [1], energy storage [2], wind turbine [3], biomass energy [4], hydrogen vehicle [5], and tidal power [6], are being further promoted. As a renewable energy technology, heat pumps acquire heat from natural sources such as ground [7], air [8], and water [9], attracting scholars' attention. Thorsteinsson et al. [10] proposed a predictive control approach for a heat pump system, reporting that the system expense could be reduced by up to 17%. Hao et al. [11] investigated a heat pump system utilizing solar energy spectral beam splitting and concluded that the system's energy efficiency could reach up to 81.7%. Chen et al. [12] found that the operating cost ($ot$) of the system could be reduced by 30.9% when a thermal energy discretization and matching approach was applied in heat pump systems. Pimm et al. [13] reported that the coefficient of performance (COP) of a high-temperature heat pump could reach up to 1.7 for industrial hydrogen demand reduction. Lee et al. [14] proposed a waste heat recovery strategy for a heat pump system, and found that the power consumption could be reduced by up to 13% when the proposed strategy was implemented. Gao et al. [15] conducted an investigation of an absorption-compression heat pump, and found that the COP decreased from 1.4 to 1.2 when the temperature increased from 70ºC to 110ºC.

Solar energy is clean and sustainable [16] and has been extensively utilized in heating systems. However, because solar irradiance is intermittent, simple heating systems with solar collectors (SCs) cannot fully satisfy the heating demand. Heat pumps can supply heat at any time of the day, but their operating costs are significantly higher than those of SCs. Solar-assisted heat pumps can address the limitations of both SCs and heat pumps. Consequently, solar-assisted heat pump systems have been widely studied. For example, Yu et al. [17] found that the COP of a solar-assisted heat pump system could be enhanced by 8.81% when the SC surface area ($A_{SC}$) increased from 1.5 $m^2$ to 3 $m^2$. Zhang et al. [18] found that the energy efficiency of a photovoltaic solar-assisted heat pump system could reach 51.39%. Gu et al. [19] conducted an experimental study of a solar-assisted heat pump system and reported that the SC efficiency and COP for the heat pump were 63% and 5.03, respectively. Song et al. [20] proposed a solar-assisted heat pump with a hybrid evaporator, finding that the system COP could reach 4.08 when there was not solar irradiance. Wang et al. [21] concluded that the payback period of a solar-assisted heat pump system was 3.86

years in comparison with the heat pump system. Chow et al. [22] investigated a solar-assisted heat pump for indoor swimming applications, and concluded that the system COP could reach 4.5, with a payback period of less than 5 years.

A water tank is an essential device in solar-assisted heat pump systems. To enhance its thermal capacity and reduce its required volume, phase change material (PCM) is usually incorporated due to its high latent heat [23]. Rahmanian et al. [24] reported that the heat transfer rate and melting rate of the PCM tank (PST) could be improved by 64.2% and 39%, respectively, when transversal oscillation was applied. Sayehvand et al. [25] concluded that the melting time of the PCM could be reduced by up to 33.8% with the use of fins in the PST. Zhang et al. [26] designed a PST with a flow channel and found that the temperature control efficiency was 47.6%. Kong et al. [27] developed a numerical model for the PST, reporting a relative error of 10.4%. Li et al. [28] analyzed the influence of different metal foam inclinations on the melting time of PST, finding that the melting time was reduced by 18.8% when the optimal metal foam inclination was applied. Meng and Zhang [29] conducted an experimental investigation of a PST, showing that with a heat transfer fluid inlet temperature at 80ºC, the charging completion time was 2,340 s and 2,220 s at flow speed of 0.15 m/s and 0.2 m/s, respectively. Liang et al. [30] concluded that the maximum effective energy efficiency was 1.3 when baffle plates were applied in the PST.

Heat loss between PST and ambient environment affects performance indicators such as the heat transfer rate, melting rate, and melting time. Therefore, it is valuable to investigate the effect of heat loss on PST performance. However, few studies have focused on the influence of heat loss on PST performance. At the system level, heat loss from PST will result in insufficient thermal energy stored to meet building heating demands, requiring additional electricity to maintain the necessary thermal energy in the PST. This, in turn, impacts the economic and environmental performance of the systems. Thus, research on the influence of heat loss from PST on energy system performance is significant. In solar-assisted heat pump systems, the PST can store thermal energy from the SC during the day and release it if needed, enhancing energy efficiency. The PST can also be used to store thermal energy from heat pumps during off-peak period and release it during on-peak period, thereby reducing $ot$. Thus, the PST is a crucial component in solar-assisted heat pump systems. As mentioned, the heat loss affects the performance of the PST, which in turn may impact the

performance of solar-assisted heat pump systems. However, few studies have examined the impact of heat loss from PST on the performance of the solar-assisted heat pump systems.

As shown in Fig. 1 (a), traditional studies primarily focused on the investigation of a single PST, often considering the influence of thermal properties and structural parameters on charging and discharging performance. Although a few studies have examined the performance of solar-assisted heat pump systems, the impact of heat loss from the PST on system performance has been neglected. This means that the extent of the impact of the heat loss from PST on the performance of the solar-assisted heat pump system remains unclear. As shown in Fig. 1 (b), the aim of this paper was to investigate the impact of heat loss from PST on the energy, economic, environmental, and technical performance. In this study, the simulation platform for the system was constructed using TRNSYS and MATLAB. The system was simulated over a period of nine years from 2003 to 2011. The comparison of the energy, economic, environmental, and technical performance between the system with and without heat loss from PST was conducted. The total electricity use ($es_t$), $ot$, carbon dioxide ($CO_2$) emission ($cn$), and thermal uncomfortable ratio ($tur$) were considered as performance indicators for the energy, economic, environmental, and technical performance, respectively. Finally, the impact of the heat loss coefficient ($h_{hl}$) on the system's energy, economic, environmental, and technical performance was analyzed.

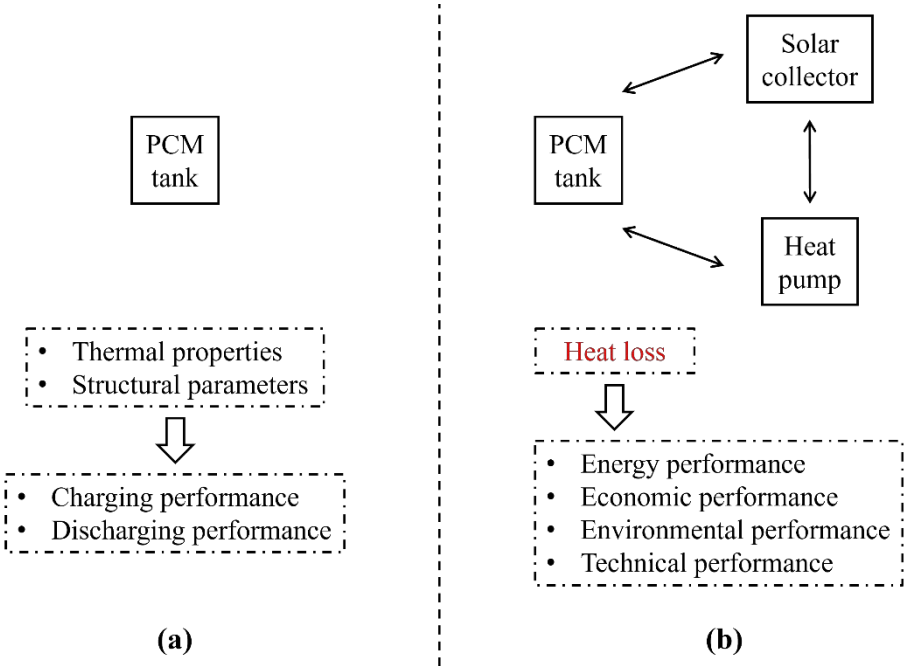

**Fig. 1.** Schematics for research strategies of (a) traditional studies and (b) this study

The novelties of this study were shown below: a) The influence of heat loss from PST on the performance of solar-assisted heat pump system was analyzed, overcoming the limitation of traditional studies that only consider effects of thermal properties and structural parameters on the performance of a single PST; b) The investigated system was applied to an open-air swimming pool, providing valuable guidance for engineers designing solar-assisted heat pump systems for swimming pool application; c) $es_t$, $ot$, $cn$, and $tur$ were selected as indicators for performance analysis of investigated system, establishing a new method for analyzing system performance across different aspects, including energy, economic, environmental, and technical performance; d) A nine-years simulation of investigated system with varying $A_{SC}$ and $h_{hl}$ was conducted, overcoming the limitation of traditional studies where performance analysis was usually carried out over a short period.

The rest of this paper is organized as the following. The methodology is presented in Section 2. Section 3 gives case study. The performance comparison between the solar-assisted heat pump systems with and without heat loss from PST is introduced in Section 4. Section 5 depicts the effect of $h_{hl}$ on the system performance. Section 6 presents the conclusions.

## 2. Methodology

Fig. 2 depicts the methodology of this study, which consists of five steps. First, a case study was selected to investigate the solar-assisted heat pump system, specifically focusing on the impact of heat loss from PST on the performance. Second, the simulation platform for the solar-assisted heat pump system was established using TRNSYS and MATLAB. Third, the performance indicators for the system analysis were identified, including energy, economic, environmental, and technical performance. Fourth, the performance of systems with and without heat loss from PST was compared. Finally, the influence of $h_{hl}$ on system performance was analyzed. The indicators identified in the third step were applied in the performance analysis during the fourth and fifth steps.

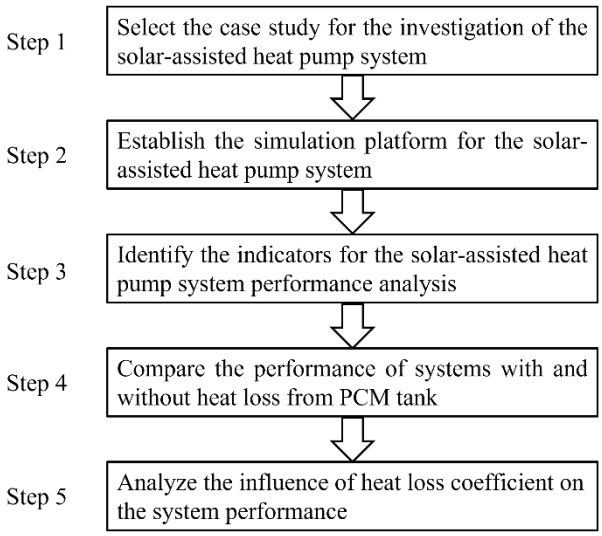


**Fig. 2.** Methodology of this study

## 3. Case study

### 3.1. Swimming pool heating application

The solar-assisted heat pump system for swimming pool heating application was selected as the case study in this research. As shown in Fig. 3, the system mainly consisted of SCs, heat exchangers (HEs), pumps, a PST, ASHPs, and a thermal-insulation cover (TIC). A detailed description of this system was provided in the study of Li et al. [2]. SCs were used to directly supply heat for the pool, while ASHPs were used to preheat the pool water and charge the PST during the electric off-peak period. The PST was used to heat the pool water during the electric on-peak period. The TIC was applied to reduce the heat loss during the closed period of the pool. The rated schedule for the pool water temperature ($T_{pw}$) is shown in Fig. 4. Detailed explanations for $T_1$, $T_2$, $T_3$, $t_1$, $t_2$, $t_3$, $t_4$, $t_5$, $t_6$, and $t_7$ were presented in the study of Li et al. [2]. $T_1$, $T_2$, and $T_3$ were set to 28.5°C, 28°C, and 26.6°C, respectively. $t_1$, $t_2$, $t_3$, $t_4$, $t_5$, $t_6$, and $t_7$ corresponded to 21:00, 5:00, 6:00, 9:00, 12:00, 18:00, and 20:00, respectively. The swimming pool where the investigated system was applied in had a surface area and volume of 1,100 $m^2$ and 1963.5 $m^3$, respectively. The system was designed to provide heat to the swimming pool during the winter season, i.e., from December 1$^{st}$ to April 30$^{th}$.

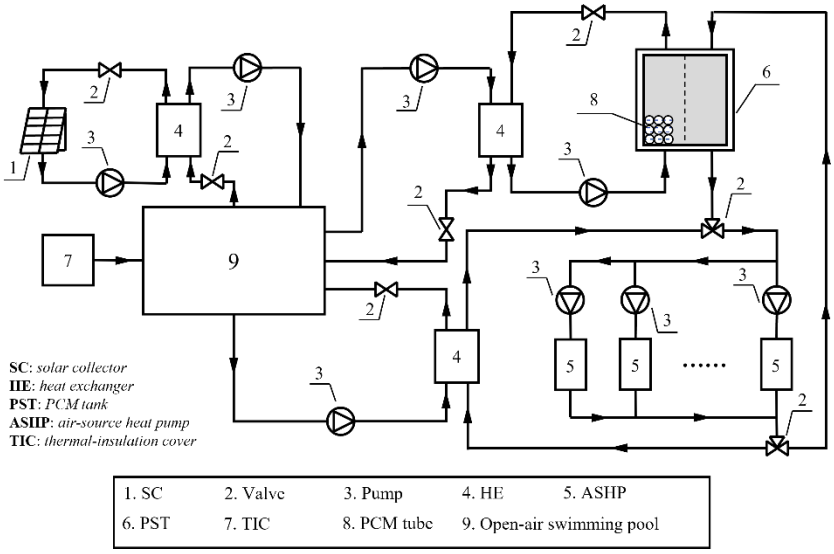


**Fig. 3.** Schematic of the solar-assisted heat pump system

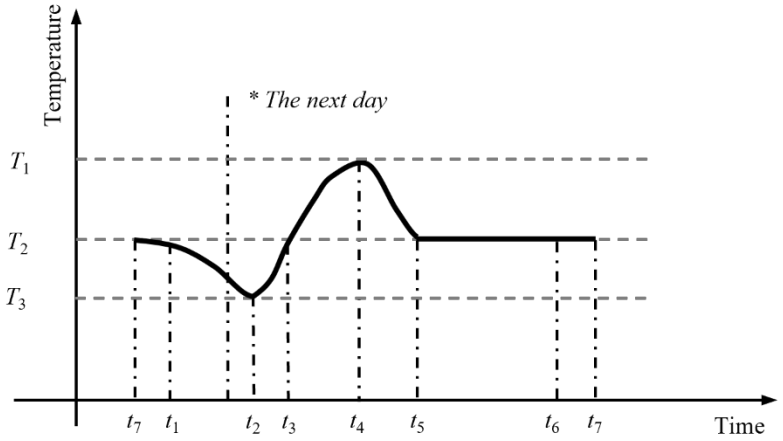


**Fig. 4.** Rated schedule of the pool water

### 3.2. System platform

TRNSYS and MATLAB were used to construct the simulation platform for the solar-assisted heat pump system. Fig. 5 depicts the simulation platform of the system. Type 941, Type 3b, Type 91, Type 649, Type 647, Type 23, and Type 71 from the TRNSYS library were used for the ASHP, pump, heat exchanger, mixing valve, diverting valve, PID controller, SC models, respectively. The experimentally validated PST and swimming pool models were developed using MATLAB program, and these models were integrated into TRNSYS using Type 155. Governing equations in water and PCM sides of PST model were respectively presented as Eqns. (1) and (2):

$$\rho_{wp}c_{wp}\epsilon\frac{\partial T_{wp}}{\partial \tau}+\rho_{wp}c_{wp}\epsilon v_{wp}\frac{\partial T_{wp}}{\partial x}=k_{wp}\epsilon\frac{\partial^2 T_{wp}}{\partial^2 x}+hv(T_{PCM}-T_{wp}) \quad (1)$$

$$\rho_{PCM}(1-\epsilon)\frac{\partial H_{PCM}}{\partial \tau}=hv(T_{wp}-T_{PCM}) \quad (2)$$

where $\rho$, $k$, $c$, $v$, $\epsilon$, and $H$ represent the density, thermal conductivity, specific heat, velocity, water fraction, and enthalpy, respectively. $wp$ represents the water in PST. $x$ and $\tau$ are the distance and time, respectively. $hv$ is the volumetric heat transfer coefficient. $T_{pw}$ during the open period could be determined by Eqn. (3):

$$\rho_{pw}c_{pw}V_{pw}\frac{dT_{pw}}{d\tau}=q_{HE}+q_{so}-q_{rs}-q_{er}-q_{cd}-q_{ra}-q_{co} \quad (3)$$

where $V_{pw}$ is the pool volume. $q_{HE}$ and $q_{so}$ are the heat from HE and solar, respectively. $q_{rs}$, $q_{er}$, $q_{cd}$, $q_{ra}$, and $q_{co}$ are the heat loss due to refilling fresh water, evaporation, conduction, radiation, convection, respectively.

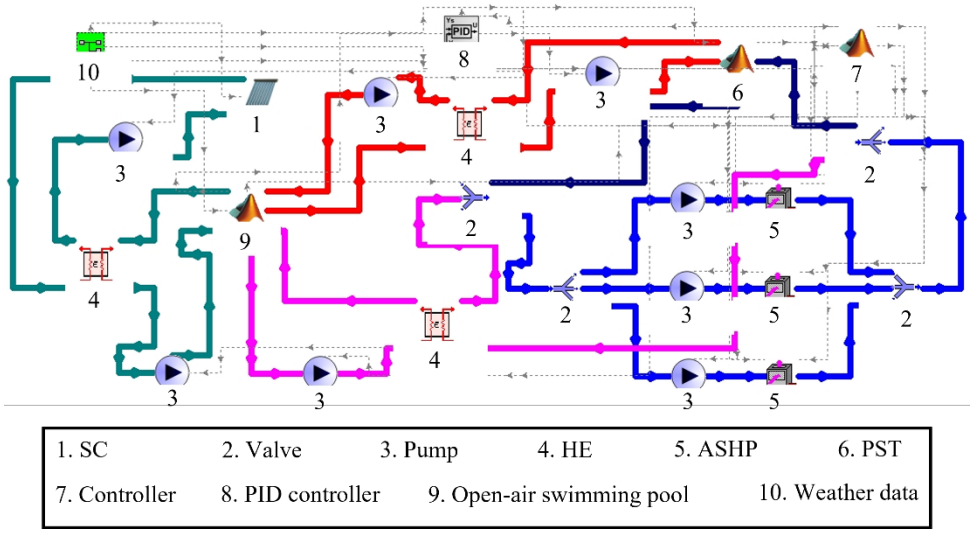


**Fig. 5.** Simulation platform of the system

The relative errors for the PST and swimming pool models were respectively 3.97% [23] and 0.5% [31], indicating that these models were accurate. Detailed information about the simulation platform was provided in the study of Li et al. [2]. Note that $T_{pw}$ varied with $\tau$, making simulation process dynamic.

### 3.3. Performance indicators

$es_t$, $ot$, $cn$, and $tur$ were chosen as the performance indicators for the energy, economic, environmental, and technical performance, respectively. $es_t$ was calculated by Eqn. (4):

$$es_t = es_a + es_p \tag{4}$$

where $a$ and $p$ denotes ASHPs and pumps, respectively. $ot$ was calculated by Eqn. (5):

$$ot = ce_{dm,ok} + ce_{ec,ok} + ce_{dm,fk} + ce_{ec,fk} \tag{5}$$

where $ce$ is the cost of electricity. $dm$, $ec$, $ok$, and $fk$ represents the demand, energy, on-peak, and off-peak periods, respectively. $cn$ was calculated by Eqn. (6):

$$cn = es_t \cdot oy \tag{6}$$

where $oy$ denotes the $CO_2$ emission coefficient for electricity. $tur$ was calculated by Eqn. (7):

$$tur = \frac{1}{t_{tl}} \int_0^{t_{tl}} um \, d\tau \tag{7}$$

where $t_{tl}$ represents the total pool open time. $um$ is a variable that was calculated by Eqn. (8):

$$um = \begin{cases} 0, & T_{pw} \geq T_s \\ 1, & T_{pw} < T_s \end{cases} \tag{8}$$

where $pw$ represents the pool water. $s$ represents the setting value. The overall performance score ($S_o$) applied in the multi-criteria optimization approach was calculated by Eqn. (9):

$$S_o = b_{es_t} \cdot S_{es_t} + b_{ot} \cdot S_{ot} + b_{ct} \cdot S_{ct} + b_{tur} \cdot S_{tur} \tag{9}$$

where $b$ represents the weight factor. $ct$ is the capital cost, which is calculated by unit cost of main components in Table 1.

**Table 1** Unit cost of main components

| Name | Unit | Cost (€/unit) |
|---|---|---|
| PST | $m^3$ | 289 |
| ASHP | kW | 148 |
| SC | $m^2$ | 94 |
| TIC | $m^2$ | 4 |
| HE | - | 702 |
| Pump | - | 597 |
| Controller | - | 2,998 |

## 4. Performance comparison between systems with and without heat loss from PST

This section presents the performance comparison between the solar-assisted heat pump systems with and without heat loss from PCM. $h_{hl}$ of PST was set as 4.55 W/($m^2$·K) [32]. The energy, economic, technical, and environmental performance of the systems with different $A_{SC}$ were analyzed. The performance of the solar-assisted heat pump system was directly related to the

weather data including dry bulb temperature, wet bulb temperature, wind speed and solar irradiance. In this study, weather data from nine different years, i.e., 2003 to 2011, were considered. These weather data were collected by Hong Kong Observatory [33]. Fig. 6 depicts the average (a) dry bulb temperature, (b) wet bulb temperature, (c) wind speed, and (d) solar irradiance in winter season from 2003 to 2011. The maximum average dry bulb temperature, wet bulb temperature, wind speed, and solar irradiance were 19.2°C, 16.8°C, 2.52 m/s, and 148 W/m$^2$, respectively. The minimum average dry bulb temperature, wet bulb temperature, wind speed, and solar irradiance were 17.8°C, 14.8°C, 2.2 m/s, and 106 W/m$^2$, respectively. The annual average system performance was also analyzed. Finally, the multi-criteria method considering energy, economic, and technical performance was applied to determine the optimal $A_{SC}$ for the systems with and without heat loss from PST.

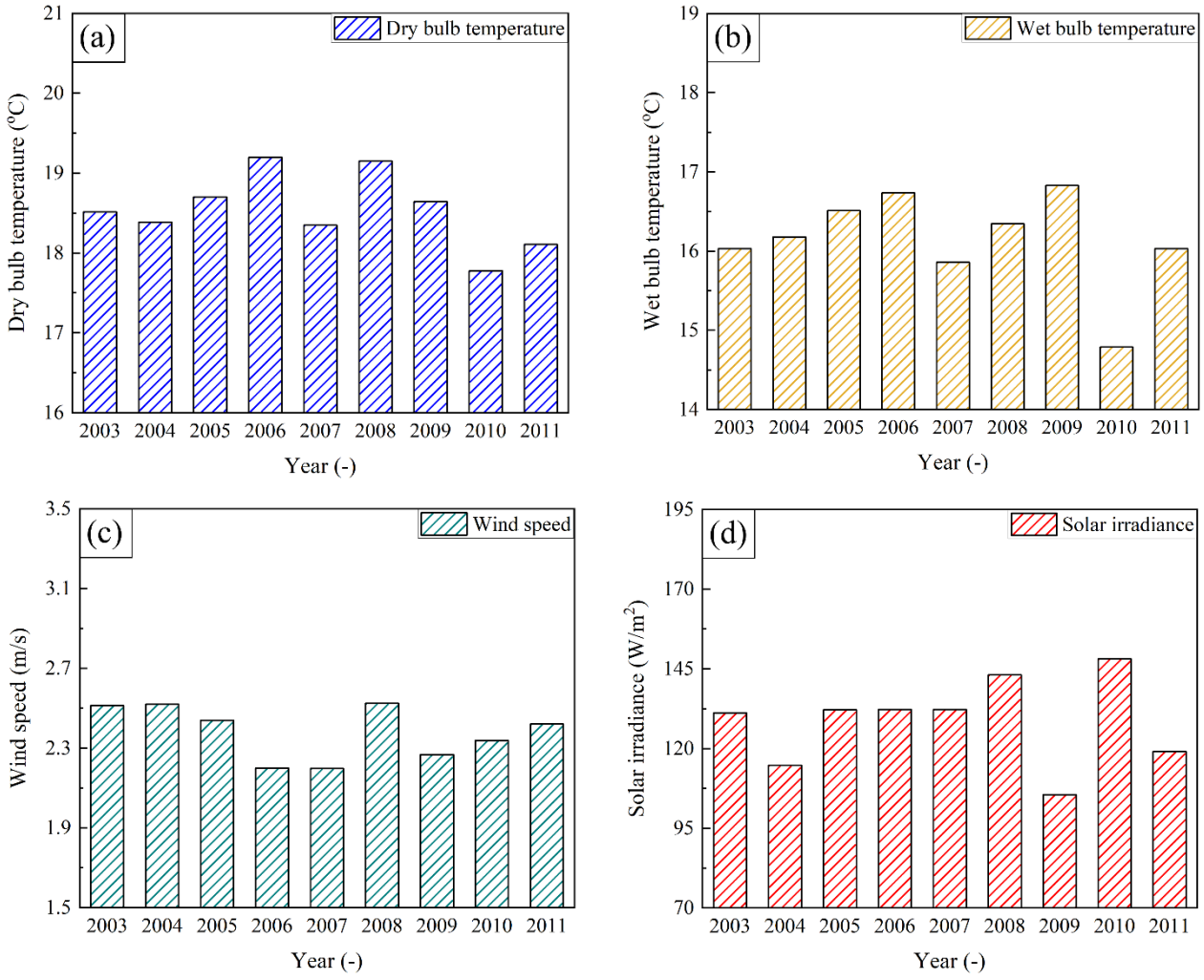

**Fig. 6.** The average (a) dry bulb temperature, (b) wet bulb temperature, (c) wind speed and (d) solar irradiance from 2003 to 2011

Fig. 7 depicts the $es_t$ comparison between the systems with and without heat loss from PST in different years. In all the years, i.e., from 2003 to 2011, the $es_t$ of the system with heat loss from PST was higher than that without heat loss from PST. In every year, $es_t$ decreased as the $A_{SC}$ increased. Increasing $A_{SC}$ allowed the SCs to adsorb more solar irradiance, leading to more heat energy supply. Consequently, the heat energy supplied by PST might be decreased, reducing the energy use of the heat pump compressor. When heat loss from PST was considered, $es_t$ in 2003, 2004, 2005, 2006, 2007, 2008, 2009, 2010, and 2011 was increased by 12.5%, 11.6%, 13.4%, 15.2%, 14.4%, 14.9%, 13.2%, 13.3%, and 12.4%, respectively. The average increase across these years was 13.4%, indicating that heat loss from PST caused a 13.4% higher energy use. As mentioned earlier, $h_{hl}$ of PST was set as 4.55 W/(m$^2$·K). This value depended on various factors, including the material and thickness of the PST's outer wall. Utilizing materials with low thermal conductivity or increasing the thickness of the wall would effectively reduce $h_{hl}$ of PST, leading to a reduction of $es_t$. Note that $A_{SC}$ ranging from 2,000 m$^2$ to 5,500 m$^2$, was applied to analyze the effect of $A_{SC}$ on system performance. An $A_{SC}$ of 5,500 m$^2$ was referenced from the study of Bawazir and Friedrich [34]. There was a case in which $A_{SC}$ was 2,500 m$^2$ and an interval of 500 m$^2$ in the study of Lisauskas [35]. Therefore, an $A_{SC}$ of 2,000 m$^2$ was chosen to represent the difference between 2,500 m$^2$ and 500 m$^2$.

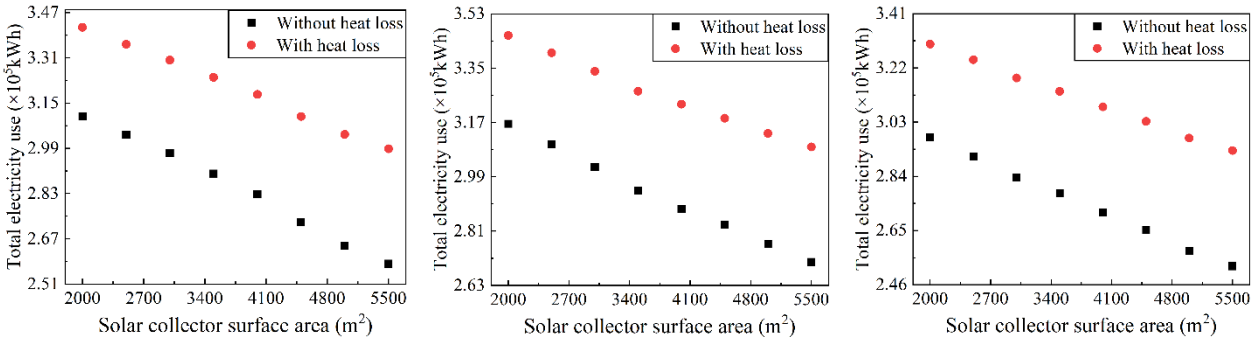


**(a)** Year 2003 **(b)** Year 2004 **(c)** Year 2005

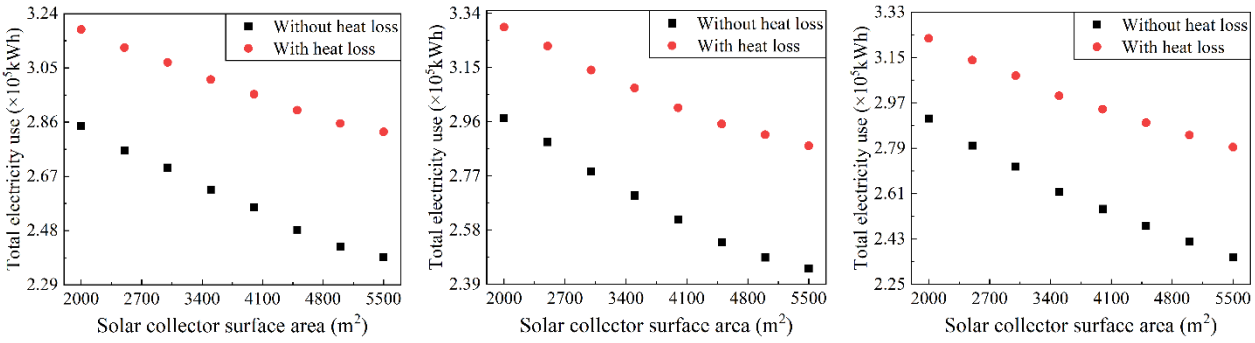


**(d)** Year 2006




**(e)** Year 2007




**(f)** Year 2008

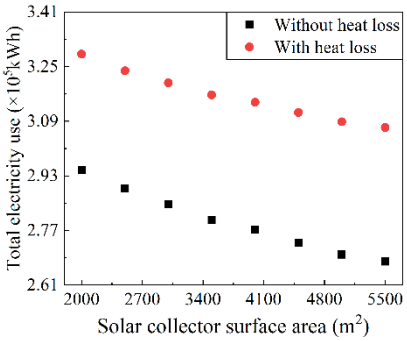


**(g)** Year 2009

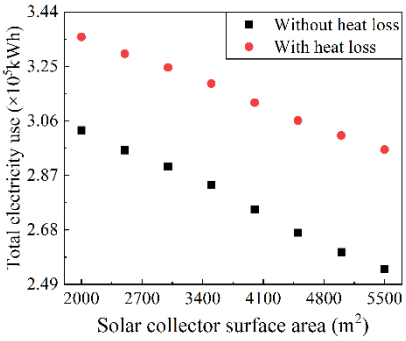


**(h)** Year 2010

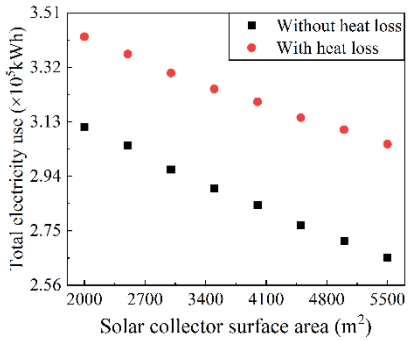


**(i)** Year 2011

**Fig. 7.** Total electricity use comparison between the systems with and without heat loss from PST in different years

Fig. 8 compares the operating cost ($ot$) between systems with and without heat loss from the PST across different years, i.e., from 2003 to 2011. In each year, the $ot$ of the system with heat loss from PST was higher than that of the system without heat loss from PST. The $ot$ decreased across all years with an increase in $A_{SC}$. As explained in Fig. 7, increasing $A_{SC}$ reduced the energy consumption of the compressor, leading to a reduction of $ot$. When accounting for heat loss from the PCM, $ot$ was increased by 9.4%, 8.7%, 9.9%, 11.2%, 10.6%, 10.9%, 9.8%, 9.9%, and 9.3% in the years 2003 through 2011. The average increase was 10%, indicating that heat loss from PST resulted in a 10% higher $ot$. Therefore, analyzing the impact of $h_{hl}$ on the economic performance of the solar-assisted heat pump system was essential, as presented in Section 5. Additionally, exploring effective measurement to enhance the economic performance of the solar-assisted heat pump system was crucial.

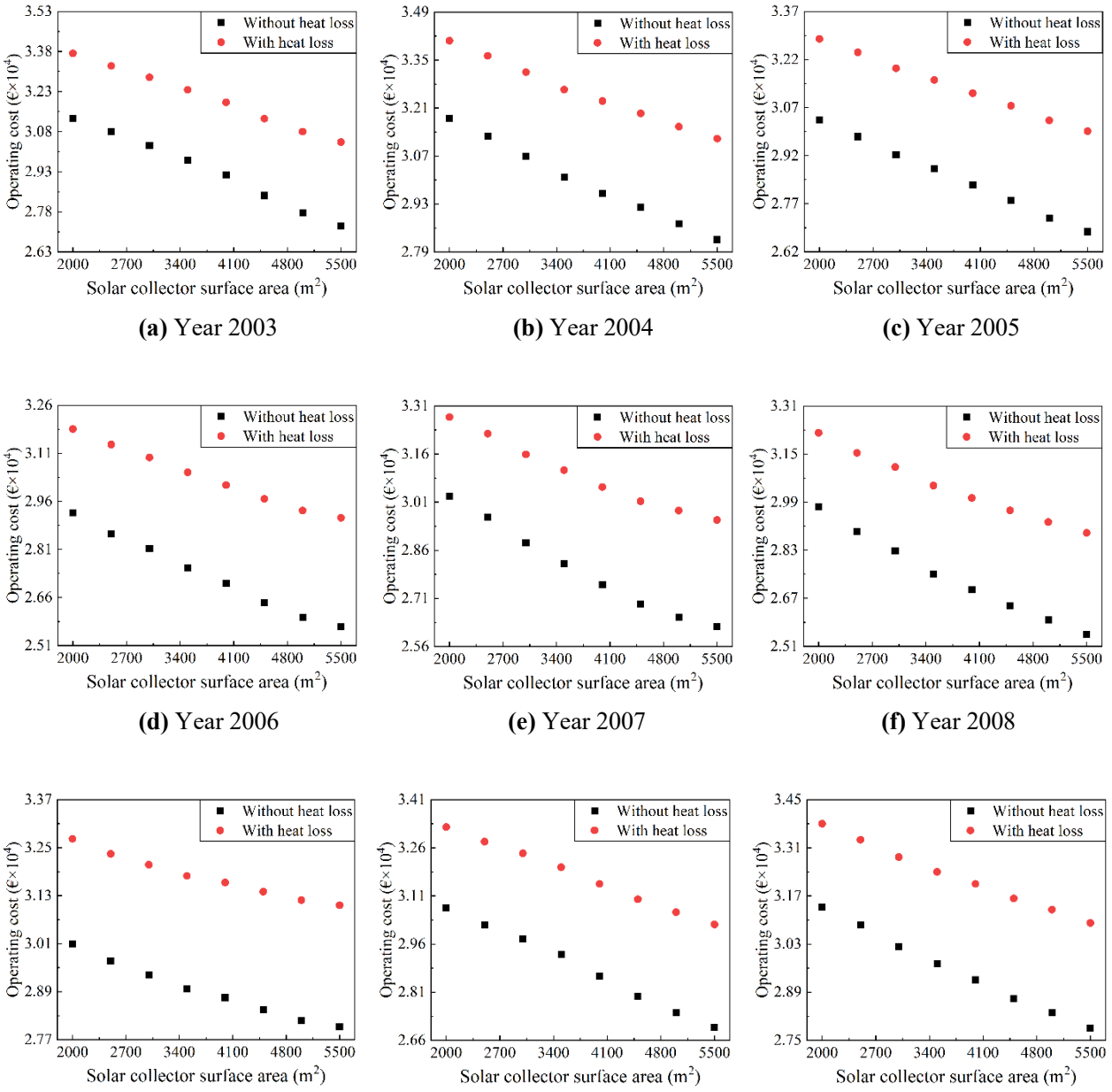


**Fig. 8.** Operating cost comparison between the systems with and without heat loss from PST in different years

Fig. 9 depicts the *tur* comparison between systems with and without heat loss from PST across different years. In 2006, 2007, 2009, and 2010, the *tur* for both systems, with and without heat loss from PST, remain 0 across various $A_{SC}$, indicating that the thermal comfort could be adequately achieved in these cases. In 2003, 2004, 2005, 2008, and 2011, however, the *tur* of the system with heat loss from PST was higher than that of system without heat loss. The variation of *tur* across different years may be attributed to differences in weather data across these years, as

shown in Fig. 6. Specifically, the maximum dry bulb temperature, wet bulb temperature, wind speed and solar irradiance occurred in 2006, 2006, 2008, and 2010, respectively, while the minimum dry bulb temperature, wet bulb temperature, wind speed and solar irradiance occurred in 2010, 2010, 2007, and 2009, respectively. These distinct weather features from 2003 to 2011 resulted in varying simulation outcomes. When considering heat loss from PST, heat was lost after the PST reached full capacity and before it could be utilized for heating, leading to situations where thermal comfort was not fully achieved. The variations of $tur$ with $A_{SC}$ were irregular. Generally, increasing $A_{SC}$ enhanced heat gain of the pool water, raising its temperature. However, in some days with low solar irradiance, the SC could not supply heat to the pool, and heat loss between the pool water and ambient temperature increased with the rising $T_{pw}$. The variability contributed to the irregular pattern of $tur$ with changes in $A_{SC}$.

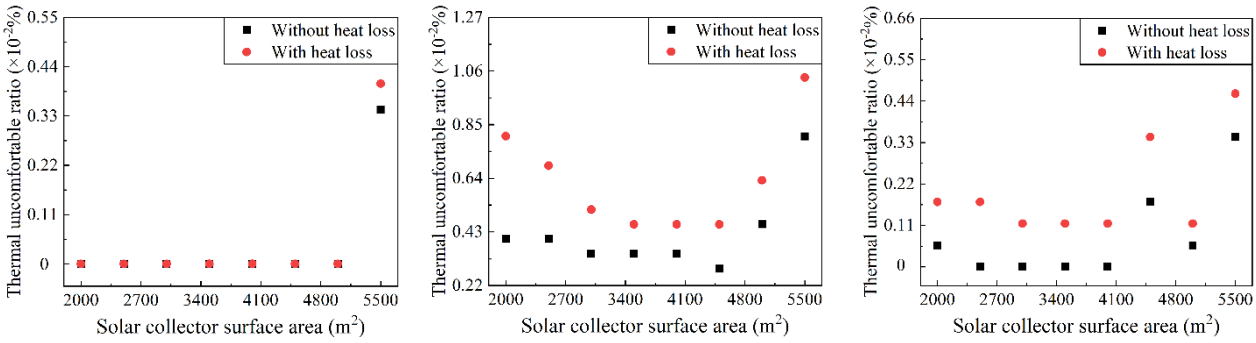


**(a)** Year 2003 **(b)** Year 2004 **(c)** Year 2005

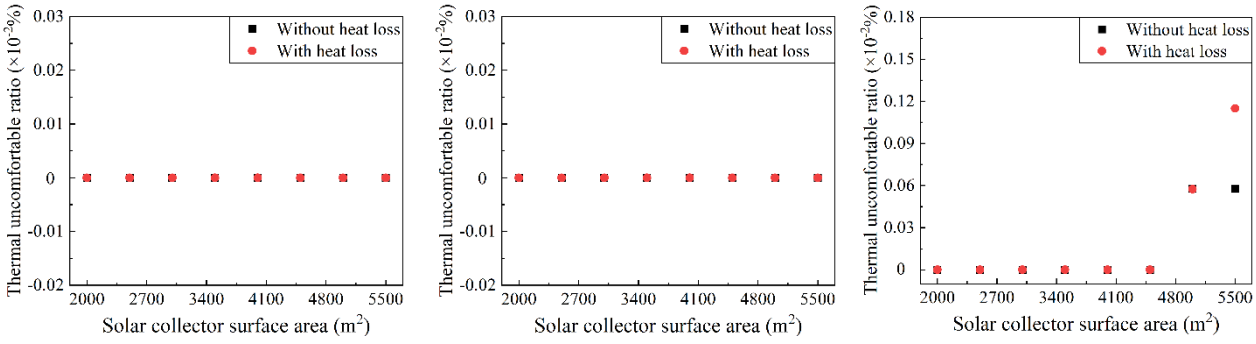


**(d)** Year 2006 **(e)** Year 2007 **(f)** Year 2008

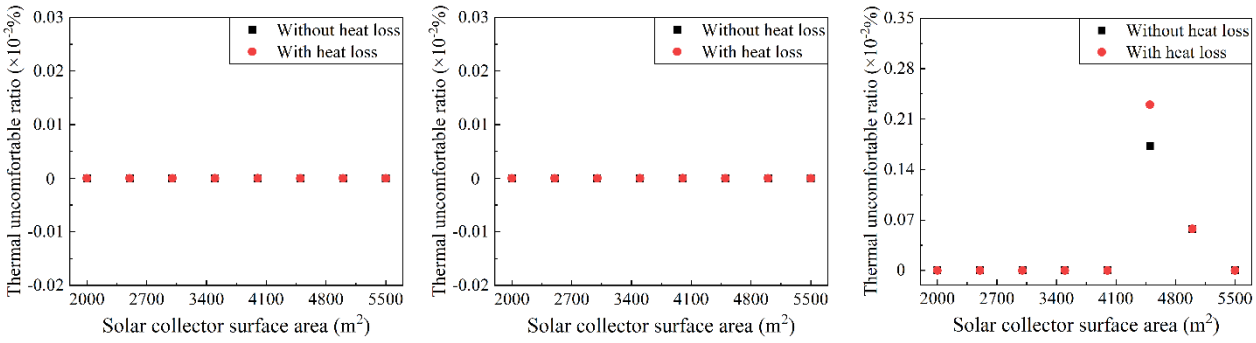


**(g)** Year 2009 **(h)** Year 2010 **(i)** Year 2011

**Fig. 9.** Thermal uncomfortable ratio comparison between the systems with and without heat loss from PST in different years

Fig. 10 depicts the $cn$ comparison between systems with and without heat loss from PST across different years. In each year, the $cn$ of the system with heat loss from PST was higher than that of system without heat loss from PST, indicating that $cn$ could be effectively reduced when the thermal insulation of the PST was maintained. $cn$ decreased across all years as $A_{ST}$ increased because $cn$ was directly related to $es_t$. As shown in Fig. 7, $es_t$ decreased as $A_{SC}$ increased, causing a reduction in $cn$ with the increase of $A_{SC}$. When heat loss from PCM was considered, the $cn$ increased by 12.5%, 11.6%, 13.4%, 15.2%, 14.4%, 14.9%, 13.2%, 13.3%, and 12.4% in the years 2003 through 2011, respectively. The average increase rate was 13.4%, meaning that heat loss from PST results in a 13.4% higher $cn$. This demonstrated that heat loss from PST significantly impacted the environmental performance of the solar-assisted heat pump system. Therefore, these results indicated that the influence of the heat loss from PST on the $cn$ of the solar-assisted heat pump system was substantial and should not be overlooked.

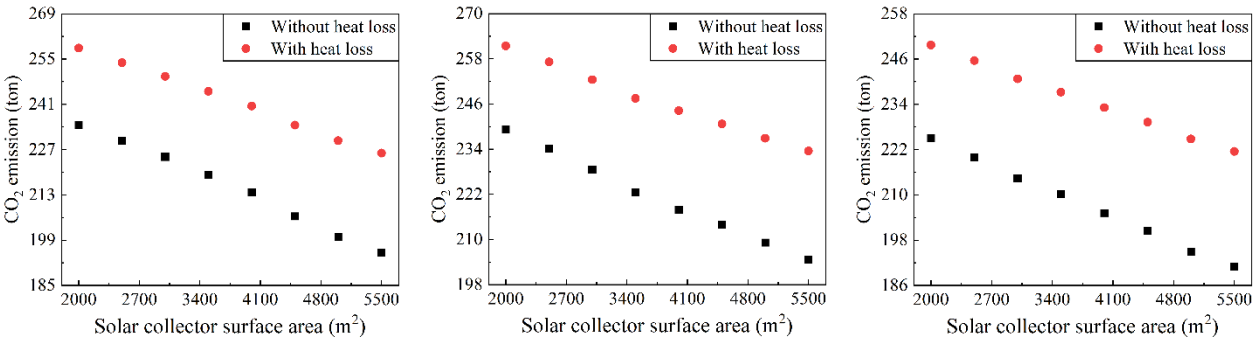


**(a)** Year 2003 **(b)** Year 2004 **(c)** Year 2005

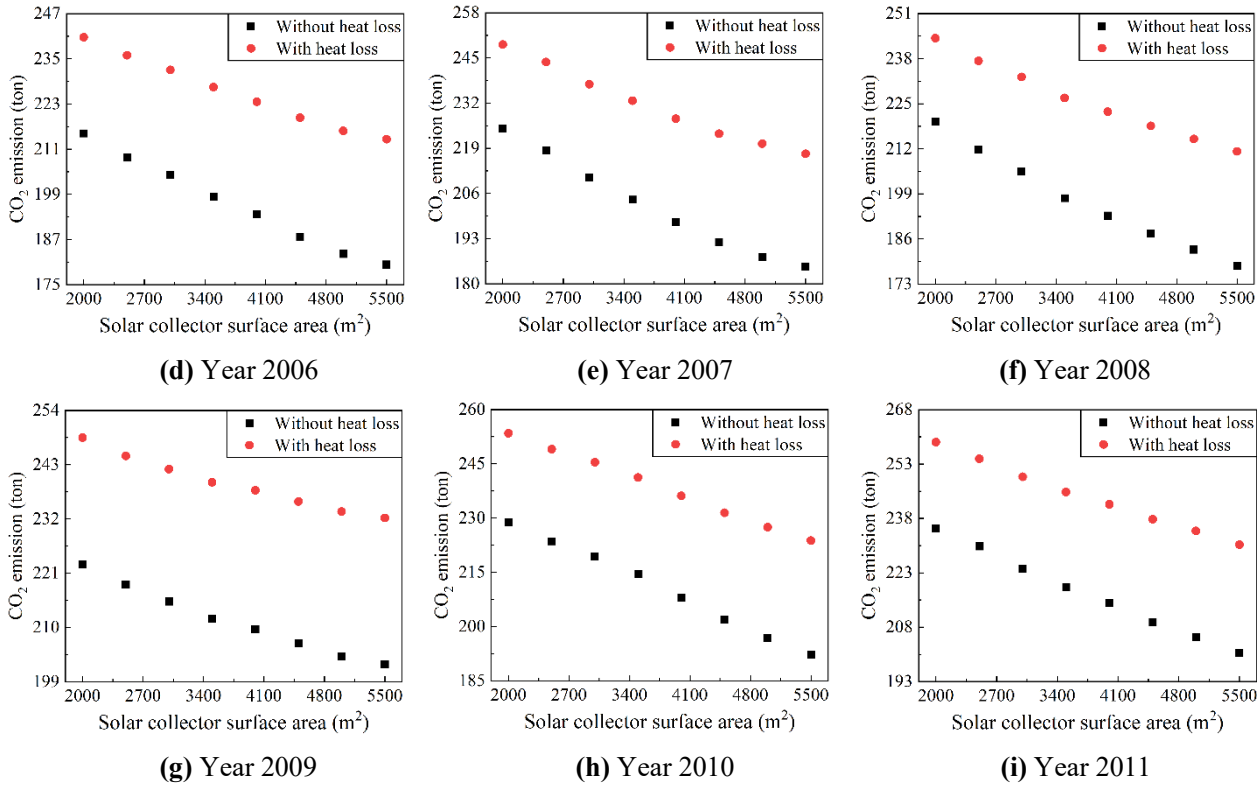


**Fig. 10.** $CO_2$ emission comparison between the systems with and without heat loss from PST in different years

Fig. 11 presents the annual average (a) $es_t$, (b) $ot$, (c) $tur$, (d) $cn$, and (e) $ct$ for systems with and without heat loss from PST. The annual average $es_t$, $ot$, $tur$, and $cn$ of the system with heat loss from PST were higher than those of the system without heat loss from PST. The explanations for the trend in the annual average $es_t$, $ot$, $tur$, and $cn$ with $A_{SC}$ were similar to those given in Figs. 7, 8, 9 and Fig. 10, respectively. The maximum annual average $es_t$ for systems with and without PST heat loss from PST were $3.33\times10^5$ kWh and $3.01\times10^5$kWh, while the minimum values were $2.95\times10^5$ kWh and $2.54\times10^5$ kWh, respectively. The average annual average $es_t$ in the systems with and without heat loss from PST were $2.78\times10^5$ kWh and $2.46\times10^5$ kWh, respectively, meaning the former was 1.13 times larger than the latter. The maximum annual average $ot$ for systems with and without heat loss from PST were € $3.3\times10^4$ and € $3.05\times10^4$, while the minimums were € $3.01\times10^4$ and € $2.7\times10^4$, respectively. The average annual average $ot$ in the systems with and without heat loss from PST were € $2.8\times10^4$ and € $2.55\times10^4$, respectively, showing a 1.1 times difference. For $tur$, the maximum annual averages with and without heat loss from PST were $2.24\times10^{-5}$ and $1.72\times10^{-5}$, while the minimums were $6.39\times10^{-6}$ and $3.83\times10^{-6}$, respectively. The average annual average $tur$ in the systems with and without heat loss from PST were $9.3\times10^{-6}$ and

$5.82\times10^{-6}$, respectively, meaning the former was 1.6 times larger than the latter. The maximum annual average $cn$ with and without heat loss from PST were 251.55 tons and 227.3 tons, while the minimums were 223.33 tons and 192.22 tons, respectively. The average annual average $cn$ in the systems with and without heat loss from PST were 210.32 tons and 185.66 tons, indicating a 1.13 times difference. In Fig. 11 (e), for both the systems, $ct$ increased with $A_{SC}$, with a maximum of € $7.7\times10^{5}$ when $A_{SC}$ was 5,500 $m^2$ and a minimum of € $4.43\times10^{5}$ when $A_{SC}$ was 2,000 $m^2$. The optimal $A_{SC}$ for $ct$ differs from that of $es_t$, $ot$, $tur$, and $cn$. Note that only the impact of heat loss from PST on the system performance was analyzed in this study, and system sizing did not consider PST heat loss. Thus, in Fig. 11 (e), $ct$ remained the same whether heat loss from PST was considered or not. Identifying the optimal SC when considering SC when $ct$, $es_t$, $ot$, $tur$, and $cn$ were simultaneously considered was challenging. Multi-criteria optimization was urgently needed to address this issue.

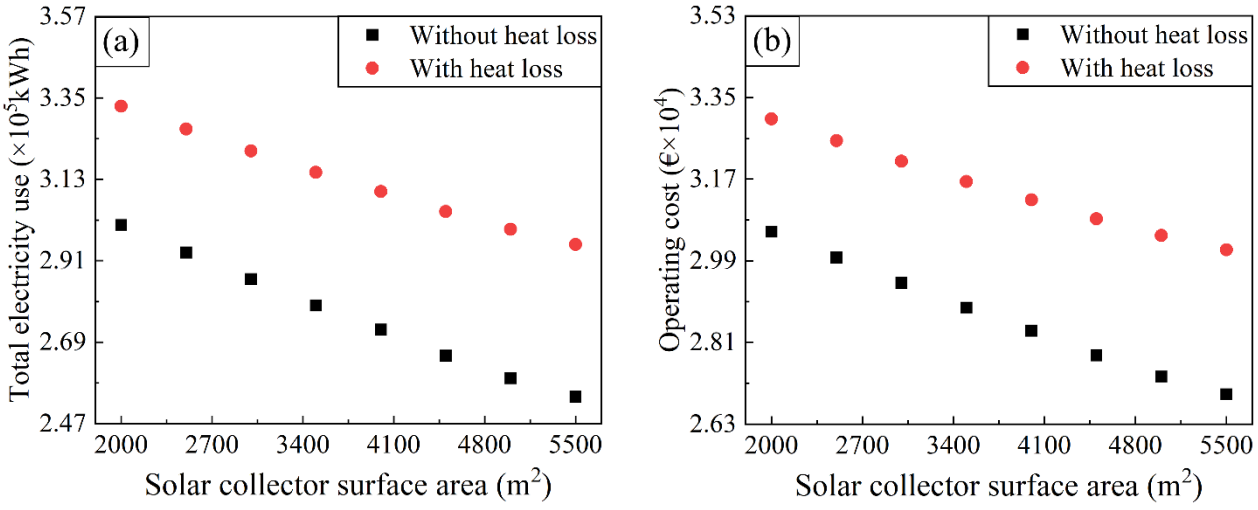

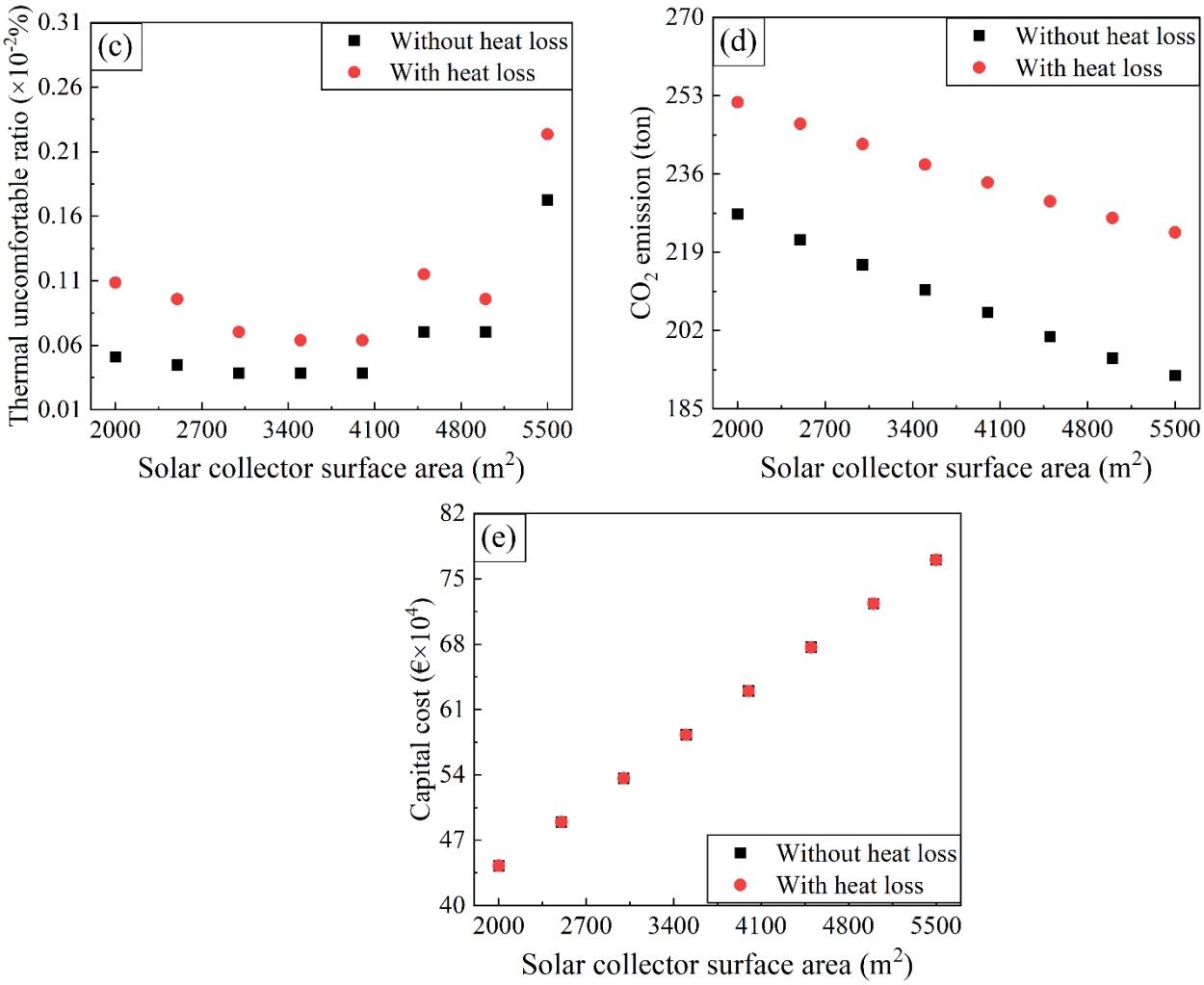


**Fig. 11.** The annual average (a) total electricity use, (b) operating cost, (c) thermal uncomfortable ratio, (d) $CO_2$ emission, and (e) capital cost of systems with and without heat loss from PST

The multi-criteria optimization approach used in the study by Li et al. [2] was applied to identify the optimal SC for solar-assisted heat pumps, both with and without the heat loss from the PST. Since $cn$ was directly related to $es_t$, $cn$ was not included in the multi-criteria optimization. The results of the optimization were influenced by the choice of the weight factors. Two scenarios with different weight factors were presented here. In the first scenario, the significance of $tur$ was equal to that of $ct$, and the significance of $ot$ was equal to that of $es_t$. The importance of the former pair was greater than that of the latter. The values of $b_{ot}$ and $b_{es_t}$ were based on the study by Li et al. [2], and thus $b_{ot}$, $b_{es_t}$, $b_{tur}$, and $b_{ct}$ were 0.2, 0.2, 0.3, and 0.3, respectively. In the second scenario, the significance of $ot$ was greater than that of $es_t$, which in turn was greater than that of $tur$. $ct$ has the smallest significance. The value of $b_{ot}$ and $b_{tur}$ were based on the study by Li et al. [2];

thus $b_{ot}$, $b_{es_t}$, $b_{tur}$, and $b_{ct}$ were 0.4, 0.3, 0.2, and 0.1, respectively. The overall performance score ($S_o$) was calculated using Eqn. (9). In Fig. 12 (a), the trend of the variation of $S_o$ with $A_{SC}$ in the system with heat loss from PST differed from that in the system without heat loss from PST. However, the difference was not significant. The optimal SC was 4,000 m$^2$ for both the systems, with and without heat loss from PST. In this case, $S_o$ was 0.68 and 0.67 for the systems with and without heat loss from PST, respectively. In Fig. 12 (b), the trend for the variation of $S_o$ with $A_{SC}$ in the system with heat loss from PST differed from that without heat loss from PST. However, the difference remained minor. The optimal SC was 5,000 m$^2$ for both the systems with and without heat loss from PST. In this case, $S_o$ was 0.8 and 0.79 for the systems with and without heat loss from PST, respectively. The difference of $S_o$ between the systems with and without heat loss from PST in Fig. 12 (a) was larger than that in Fig. 12 (b), indicating that this difference was related to the weight factors of $ot$, $es_t$, $tur$, and $ct$. In some cases, specific weight factors might result in a greater difference in $S_o$, which might cause the optimal $A_{SC}$ to vary between systems with and without heat loss from PST.

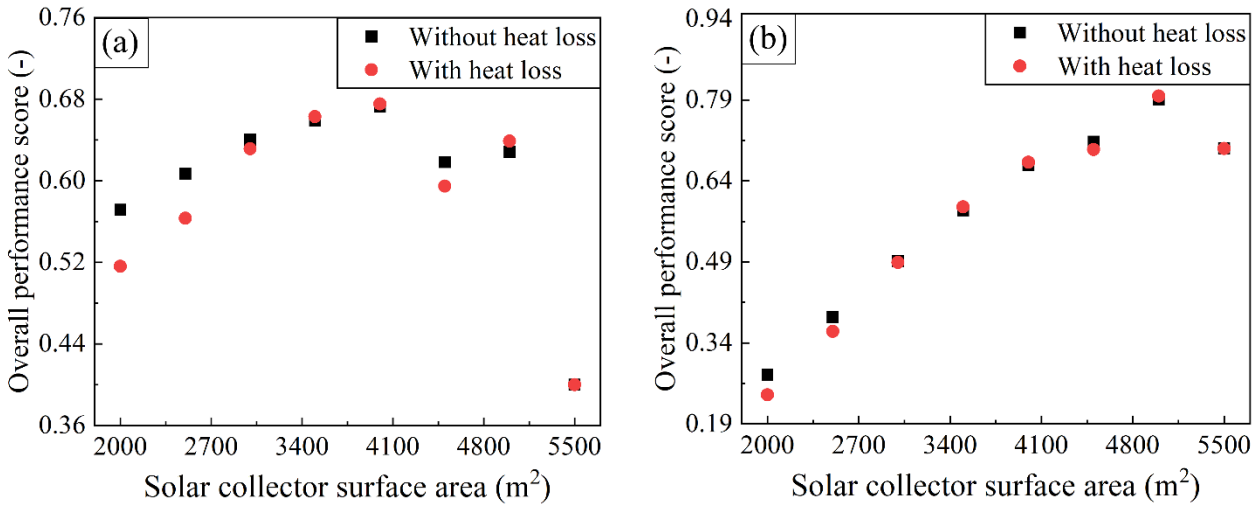


**Fig. 12.** Variations of overall performance score with SC surface area when weighting factors of $ot$, $es_t$, $tur$, and $ct$ were (a) 0.2, 0.2, 0.3, and 0.3; (b) 0.4, 0.3, 0.2, and 0.1

## 5. Effect of heat loss coefficient

This section presents the effect of different $h_{hl}$ on system performance, including energy, economic, technical, and environmental aspects. The system performance over nine years, i.e., from 2003 to 2011, was considered. The annual average system performance was also analyzed.

Fig. 13 depicts the variations of $es_t$ with different $h_{hl}$ across various years. In every year, $es_t$ increased as $h_{hl}$ increased, regardless of whether $A_{SC}$ was 2,000 $m^2$, 3,000 $m^2$, or 4,000 $m^2$, indicating that more electricity would be consumed when a higher $h_{hl}$ was considered. The trend for the variation of $es_t$ with $h_{hl}$ was linear. The results in Fig. 13 showed that approximately 20% more energy would be utilized when $h_{hl}$ increased from 2 W/($m^2$·K) to 12 W/($m^2$·K). Note that the range of $h_{hl}$, from 2 W/($m^2$·K) to 12 W/($m^2$·K), was chosen to analyze its effect on system performance. The value of 2 W/($m^2$·K) referred to the study of Melo and Lamberts [36], while 12 W/($m^2$·K) referred to the study of Jin et al. [37].

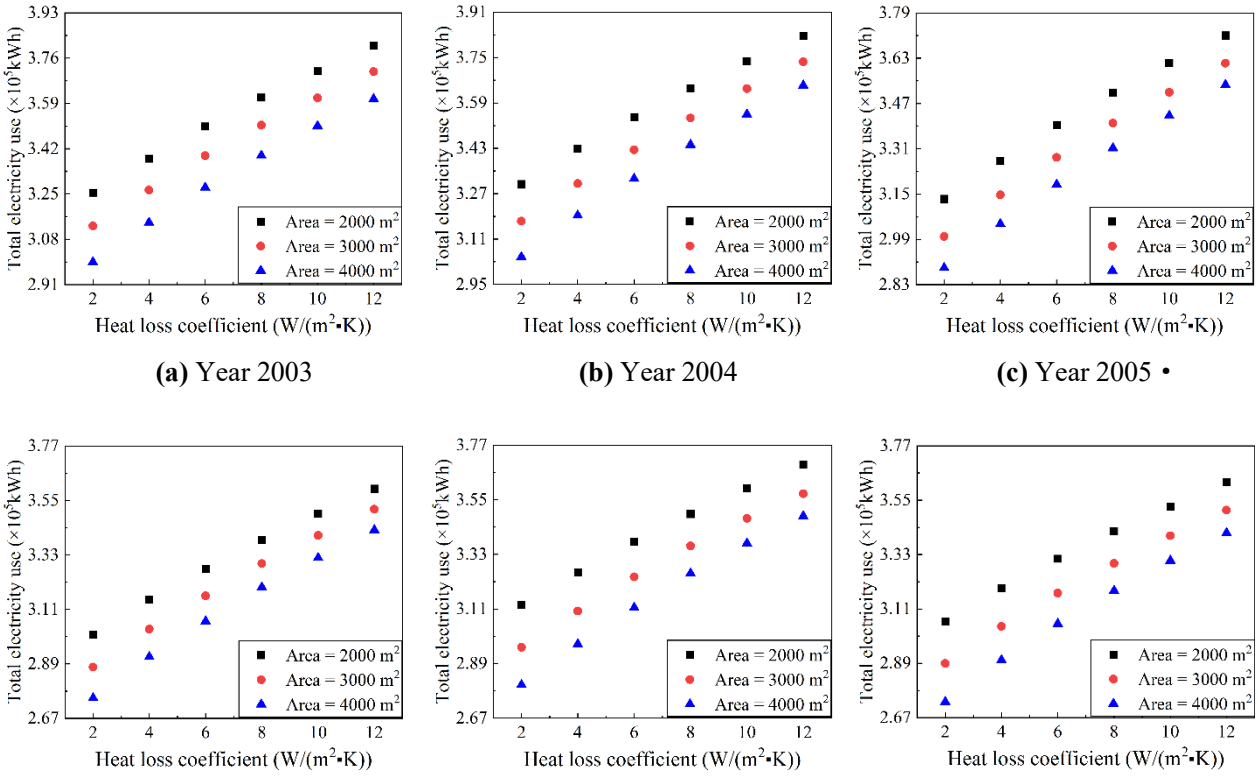


**(a)** Year 2003 **(b)** Year 2004 **(c)** Year 2005 •

**(d)** Year 2006 **(e)** Year 2007 **(f)** Year 2008

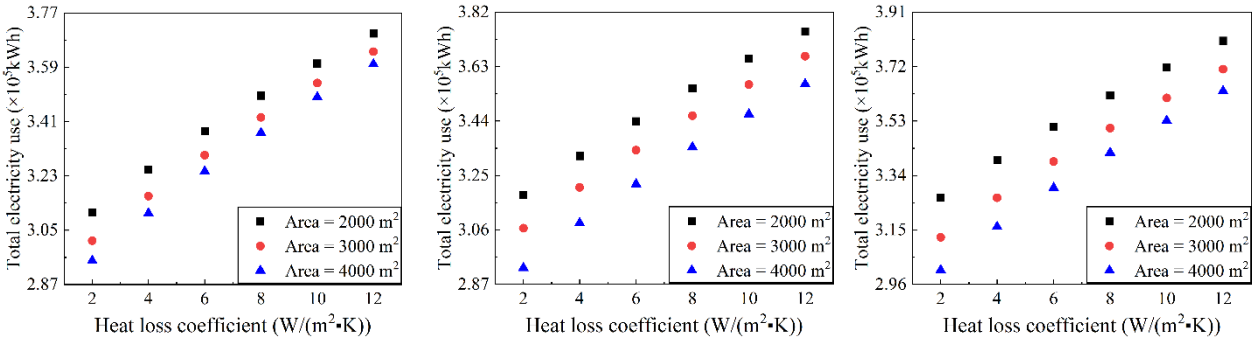


**(g)** Year 2009 **(h)** Year 2010 **(i)** Year 2011

**Fig. 13.** Variations of total electricity use with different heat loss coefficients in different years

Fig. 14 depicts the variations of $ot$ with different $h_{hl}$ across various years. In each year, $ot$ increased as $h_{hl}$ increased, regardless of whether $A_{SC}$ was 2,000 $m^2$, 3,000 $m^2$, or 4,000 $m^2$, indicating that higher $ot$ was incurred when a higher $h_{hl}$ was considered. The trend for the variation of $ot$ with $h_{hl}$ was linear. The results in Fig. 14 showed that $ot$ would be approximately 15% higher when $h_{hl}$ increased from 2 W/($m^2$·K) to 12 W/($m^2$·K).

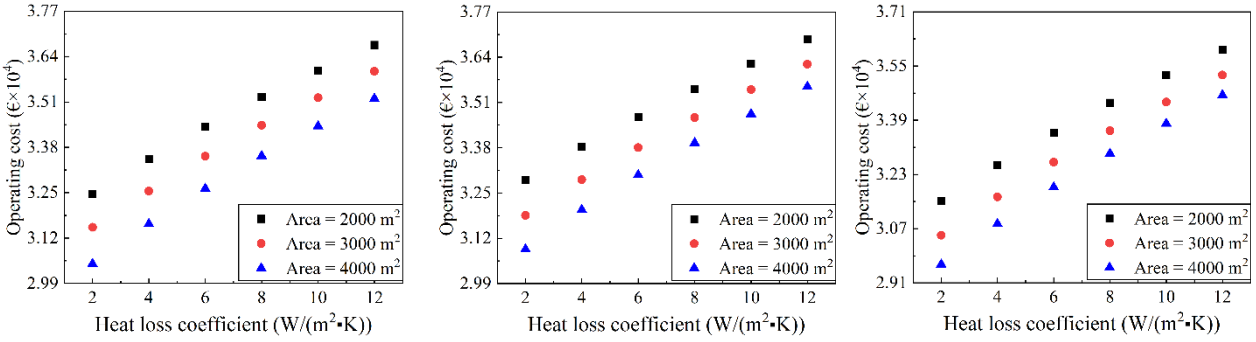


**(a)** Year 2003 **(b)** Year 2004 **(c)** Year 2005

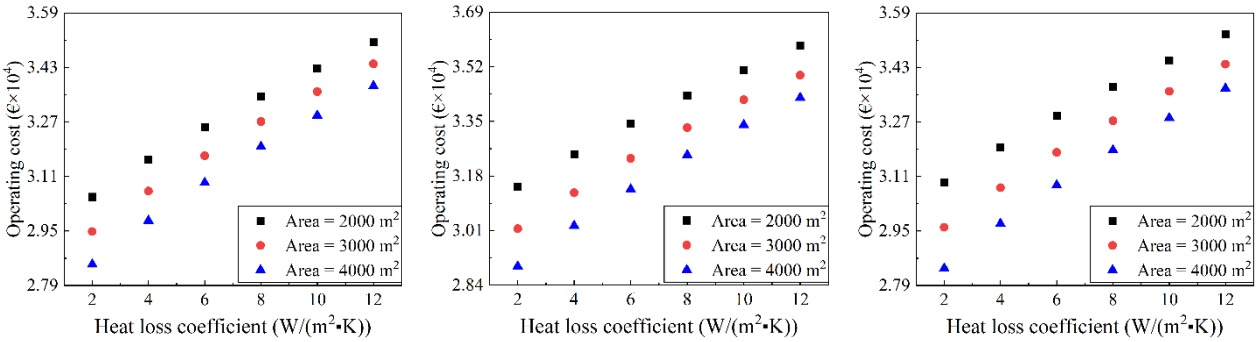


**(d)** Year 2006 **(e)** Year 2007 **(f)** Year 2008

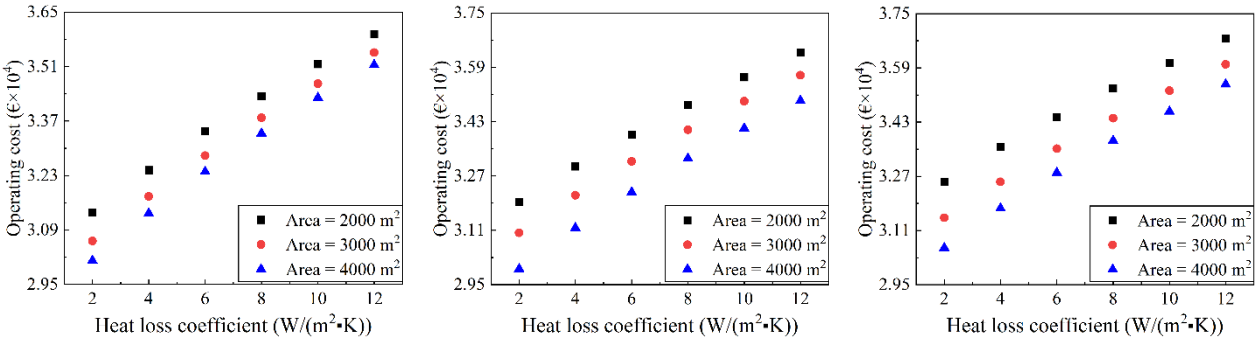


**(g)** Year 2009 **(h)** Year 2010 **(i)** Year 2011

**Fig. 14.** Variations of operating cost with different heat loss coefficients in different years

Fig. 15 depicts the variations of *tur* with different $h_{hl}$ across various years. In 2003, 2006, 2007, 2008, 2009, 2010, and 2011, *tur* remained 0 as $h_{hl}$ increased from 2 W/(m$^2$·K) to 12 W/(m$^2$·K). However, in 2004 and 2005, *tur* increased as $h_{hl}$ increased, regardless of whether $A_{SC}$ was 2,000 m$^2$, 3,000 m$^2$, or 4,000 m$^2$, meaning that the stored heat might not be sufficient to meet heating demands with the increase of heat loss from PST. For an $A_{SC}$ of 2,000 m$^2$, the maximum *tur* in 2004 and 2005 were $1.4\times10^{-4}$ and $4.02\times10^{-5}$, respectively, occurring when $h_{hl}$ was 12 W/(m$^2$·K). The minimum *tur* in these years were $5.17\times10^{-5}$ and $1.15\times10^{-5}$, respectively, occurring when $h_{hl}$ was 2 W/(m$^2$·K). For an $A_{SC}$ of 3,000 m$^2$, the maximum *tur* in 2004 and 2005 were $1.15\times10^{-4}$ and $3.4\times10^{-5}$, respectively, occurring when $h_{hl}$ was 12 W/(m$^2$·K). The minimum *tur* in these years were $4\times10^{-5}$ and $6\times10^{-6}$, respectively, occurring when the heat loss was 2 W/(m$^2$·K). For an $A_{SC}$ of 4,000 m$^2$, the maximum *tur* in 2004 and 2005 were $1.09\times10^{-4}$ and $2.9\times10^{-5}$, respectively, occurring when $h_{hl}$ was 12 W/(m$^2$·K). The minimum *tur* in these years were $4\times10^{-5}$ and 0, respectively, occurring when the heat loss was 2 W/(m$^2$·K). These results indicated that thermal comfort requirements were significantly compromised as $h_{hl}$ increased from 2 W/(m$^2$·K) to 12 W/(m$^2$·K).

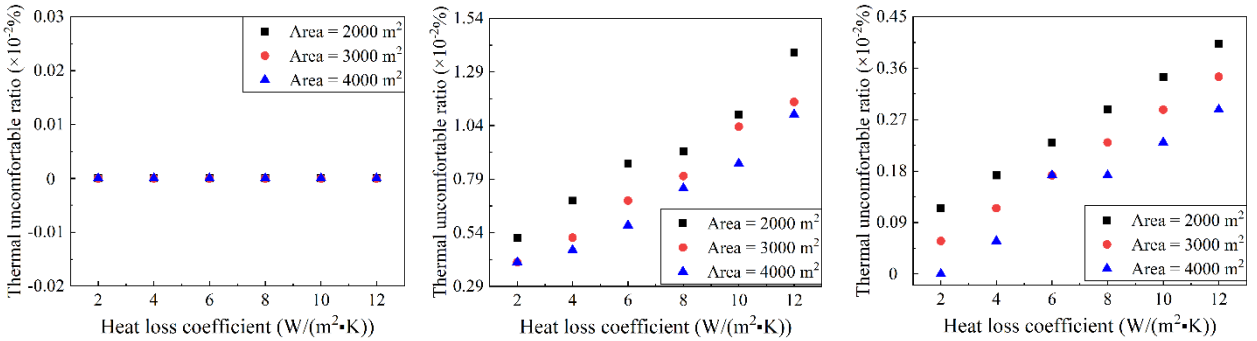


**(a)** Year 2003 **(b)** Year 2004 **(c)** Year 2005

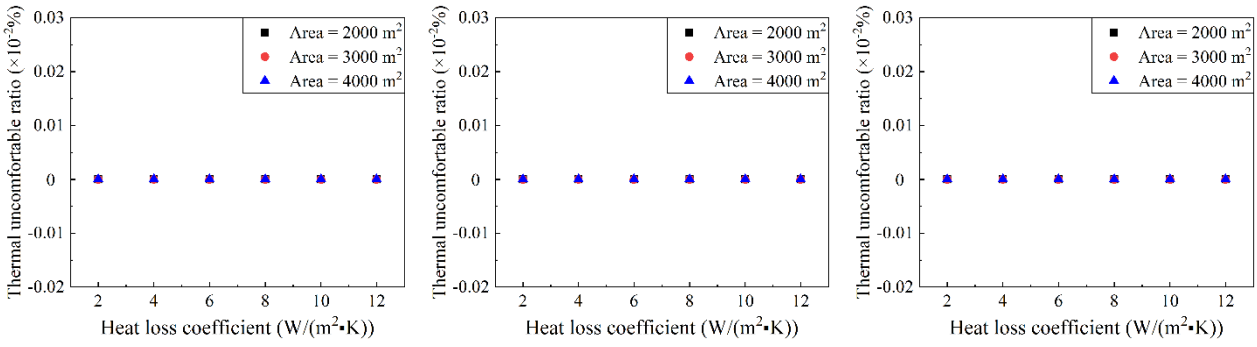


**(d)** Year 2006 **(e)** Year 2007 **(f)** Year 2008

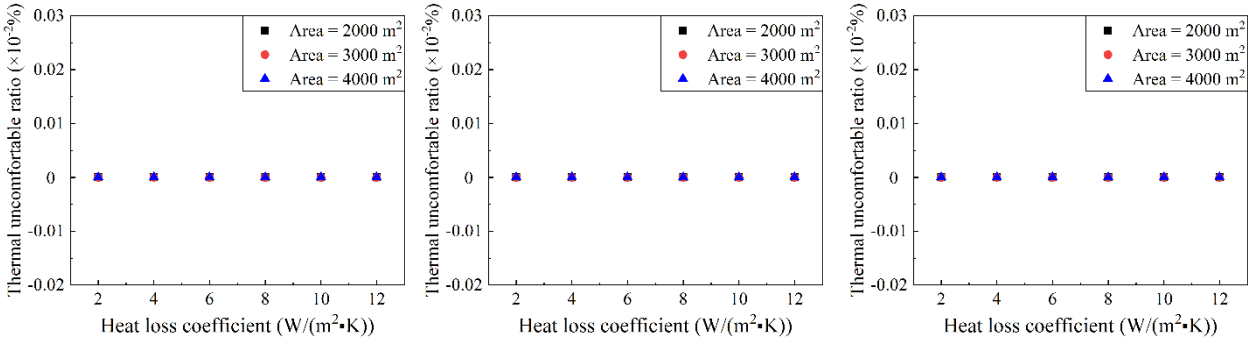


**(g)** Year 2009 **(h)** Year 2010 **(i)** Year 2011

**Fig. 15.** Variations of thermal uncomfortable ratio with different heat loss coefficients in different years

Fig. 16 depicts the variations of $cn$ with different $h_{hl}$ across various years. In each year, $cn$ increased as $h_{hl}$ increased, regardless of whether $A_{SC}$ was 2,000 m$^2$, 3,000 m$^2$, or 4,000 m$^2$, meaning that higher $h_{hl}$ led to greater $cn$. The trend for the variation of $cn$ with $h_{hl}$ was linear. Analysis of the Fig. 16 showed that $cn$ would increase by approximately 20% when $h_{hl}$ increased from 2 W/(m$^2$·K) to 12 W/(m$^2$·K).

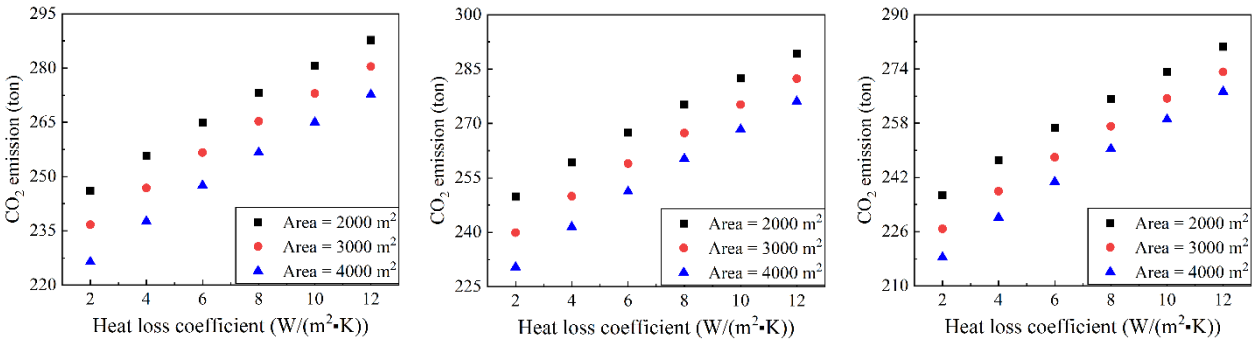


**(a)** Year 2003 **(b)** Year 2004 **(c)** Year 2005

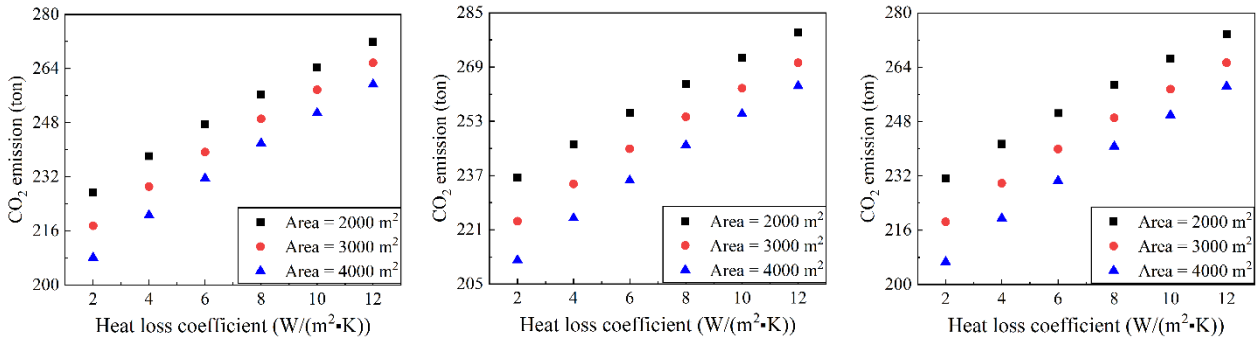


**(d)** Year 2006 **(e)** Year 2007 **(f)** Year 2008

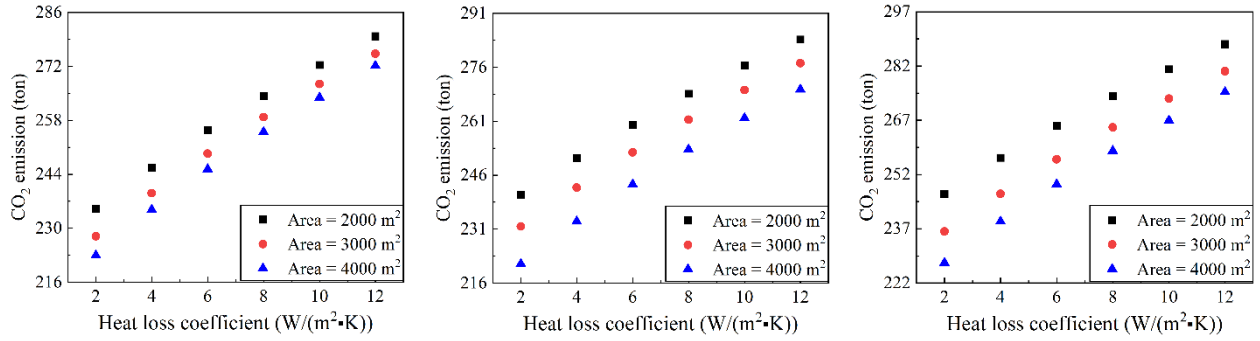


**(g)** Year 2009 **(h)** Year 2010 **(i)** Year 2011

**Fig. 16.** Variations of $CO_2$ emission with different heat loss coefficients in different years

Fig. 17 depicts the variations of the annual average (a) $es_t$, (b) $ot$, (c) $tur$, and (d) $cn$ for systems with different $h_{hl}$. The annual average $es_t$, $ot$, $tur$, and $cn$ increased as the $h_{hl}$ rose. The analysis of these variations aligned with the analysis for the Figs. 13, 14, 15, and 16. For the case where $A_{SC}$ was 2,000 m$^2$, $es_t$ was 3.16×10$^5$ kWh when $h_{hl}$ was 2 W/(m$^2$·K) and increased to 3.72×10$^5$ kWh when $h_{hl}$ reached 12 W/(m$^2$·K), representing a 17.9% increase. The $ot$ was € 3.17×10$^4$ at $h_{hl}$ of 2 W/(m$^2$·K) and rose to € 3.61×10$^4$ at $h_{hl}$ of 12 W/(m$^2$·K), representing a 13.7% increase. The $tur$ was 7×10$^{-6}$ at $h_{hl}$ of 2 W/(m$^2$·K) and rose to 1.98×10$^{-5}$ at $h_{hl}$ of 12 W/(m$^2$·K), representing a 181.8% increase. The $cn$ was 238.9 tons at $h_{hl}$ of 2 W/(m$^2$·K) and rose to 281.6 tons at $h_{hl}$ of 12 W/(m$^2$·K), representing a 17.9% increase.

For the case where $A_{SC}$ was 3,000 m$^2$, $es_t$ was 3.03×10$^5$ kWh at $h_{hl}$ of 2 W/(m$^2$·K) and rose to 3.63×10$^5$ kWh at $h_{hl}$ of 12 W/(m$^2$·K), representing a 20% increase. The $ot$ was € 3.07×10$^4$ at $h_{hl}$ of 2 W/(m$^2$·K) and rose to € 3.54×10$^4$ at $h_{hl}$ of 12 W/(m$^2$·K), representing a 15.2% increase. The $tur$ was 5.1×10$^{-6}$ at $h_{hl}$ of 2 W/(m$^2$·K) and rose to 1.66×10$^{-5}$ at $h_{hl}$ of 12 W/(m$^2$·K), representing

a 225% increase. The $cn$ was 228.7 tons at $h_{hl}$ of 2 W/(m$^2$·K) and rose to 274.5 tons at $h_{hl}$ of 12 W/(m$^2$·K), representing a 20% increase.

For the case where $A_{SC}$ was 4,000 m$^2$, $es_t$ was 2.9×10$^5$ kWh at $h_{hl}$ of 2 W/(m$^2$·K) and rose to 3.55×10$^5$ kWh at $h_{hl}$ of 12 W/(m$^2$·K), representing a 22.3% increase. The $ot$ was € 2.97×10$^4$ at $h_{hl}$ of 2 W/(m$^2$·K) and rose to € 3.47×10$^4$ at $h_{hl}$ of 12 W/(m$^2$·K), representing a 16.8% increase. The $tur$ was 4.5×10$^{-6}$ at $h_{hl}$ of 2 W/(m$^2$·K) and rose to 1.53×10$^{-5}$ at $h_{hl}$ of 12 W/(m$^2$·K), representing a 242.9% increase. The $cn$ was 219.3 tons at $h_{hl}$ of 2 W/(m$^2$·K) and rose to 268.2 tons at $h_{hl}$ of 12 W/(m$^2$·K), representing a 22.3% increase.

When $h_{hl}$ increased from 2 W/(m$^2$·K) to 12 W/(m$^2$·K), the increase of $es_t$, $ot$, $tur$, and $cn$ reached up to 22.3%, 16.8%, 242.9%, and 22.3%, respectively. This indicated that each additional 1 W/(m$^2$·K) would lead to increases of 2.23%, 1.68%, 24.3%, and 2.23% for $es_t$, $ot$, $tur$, and $cn$, respectively. These values highlighted the significance of $h_{hl}$ for maintaining optimal performance in solar-assisted heat pump systems. Improved thermal-insulation of the PST could reduce $h_{hl}$, thereby enhancing the energy, economic, environmental, and technical performance.

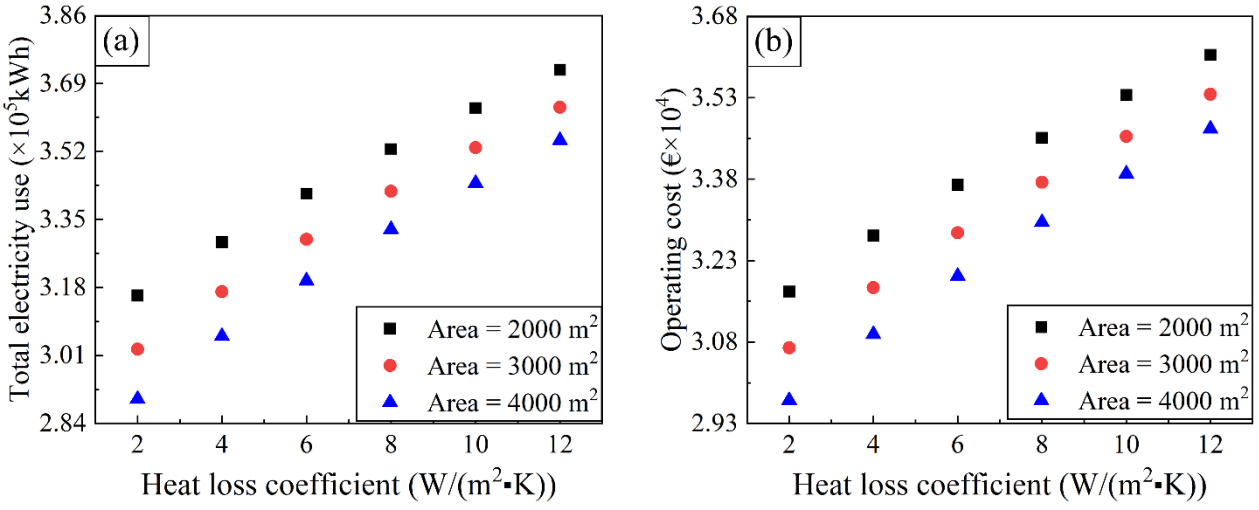

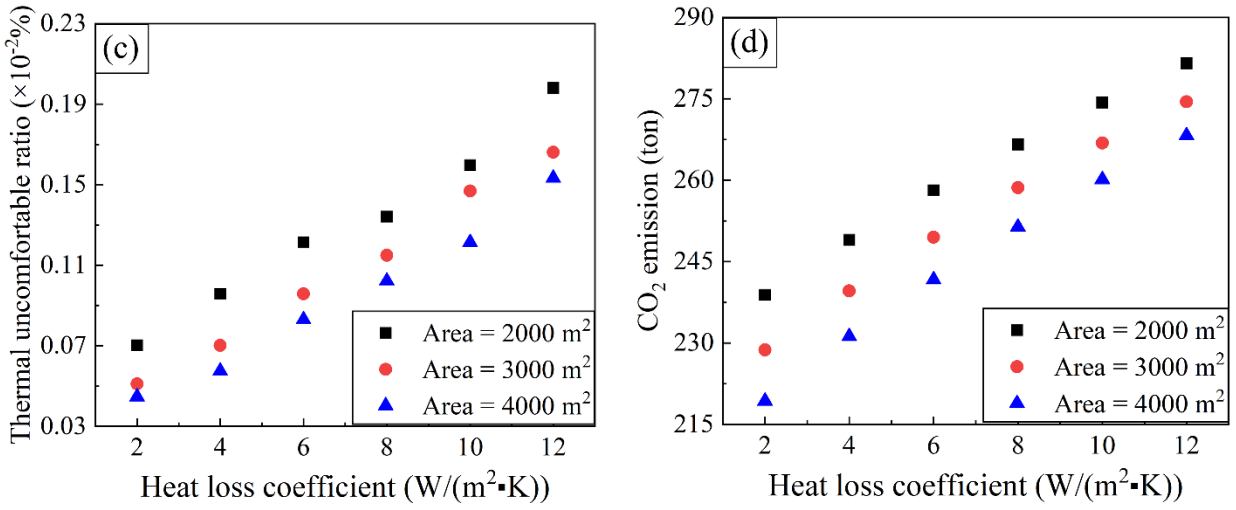


**Fig. 17.** The variations of the average (a) total electricity use, (b) operating cost, (c) thermal uncomfortable ratio, and (d) $CO_2$ emission with different heat loss coefficients

## 6. Conclusions

This study examined the impact of heat loss from PST on the performance of a solar-assisted heat pump system. A case study was conducted where the solar-assisted heat pump system with the PST was used to supply heat to a swimming pool. TRNSYS and MATLAB were used to construct the system's simulation platform. $es_t$, $ot$, $cn$, and $tur$ served as the performance indicators for energy, economic, environmental, and technical performance, respectively.

The study compared system performance with and without heat loss from PST and analyzed the influence of $h_{hl}$ on system performance. The average annual average $es_t$ for systems with and without heat loss from PST was $2.78\times10^5$ kWh and $2.46\times10^5$ kWh, respectively. Correspondingly, the energy use per area was 252.9 kWh/m$^2$ with heat loss from PST and 223.6 kWh/m$^2$ without heat loss from PST, indicating a 13.3% higher energy consumption due to heat loss from PST. The average annual average $ot$ for systems with and without heat loss from PST was € $2.8\times10^4$ and € $2.55\times10^4$, respectively, resulting in a 9.9% higher cost with heat loss from PST. The average annual average $tur$ for systems with and without heat loss from PST was $9.3\times10^{-6}$ and $5.82\times10^{-6}$, respectively, meaning the former was 1.6 times larger than the latter. The optimal $A_{SC}$, identified via multi-criteria optimization approach, was the same for systems with and without PST heat loss, though variations in weight factors could lead to different optimal SC values. As $h_{hl}$ increased from 2 W/(m$^2$·K) to 12 W/(m$^2$·K), the increases of $es_t$, $ot$, $tur$, and $cn$ could reach 22.3%, 16.8%,

242.9%, and 22.3%, respectively. These results highlighted the significance of the thermal insulation for the PST. This study addressed the extent of the influence of heat loss from PST on the performance of solar-assisted heat pump system.

The key limitations of this study were as follows: a) A photovoltaic/thermal collector could be used instead of a solar collector, potentially enhancing the energy efficiency. Therefore, a feasibility study on using PV/T collectors for swimming pool applications should be conducted.; b) Currently the investigated system was utilized to heat the swimming pool during winter season, meaning it remained idle during other seasons. Extending the system's application to other uses, such as providing domestic hot water, and evaluating its year-round performance would be beneficial; c) The use of SC could effectively increase energy efficiency but also raise system's $ct$. Therefore, it was necessary to compare the performance between systems with and without SC comprehensively; d) During the system's operation, temperature setpoints $T_1$ and $T_2$ were controlled to maintain desired levels. However, the effects of $T_1$ and $T_2$ on the energy, economic, and technical performance remained unclear. Future studies should analyze how $T_1$ and $T_2$ impacted system performance.

**Acknowledgements**

This work is supported by Guangdong Basic and Applied Basic Research Foundation (2022A1515140105) and Guangdong Provincial University Youth Innovative Talent Project (2024KQNCX154). This work is also supported by Guangdong Provincial University Innovation Team Project, No.2023KCXTD038. This project has received funding from the European Union's Horizon 2020 research and innovation programme under the Marie Skłodowska-Curie grant agreement No [895732].

**Appendix A**

Fig. A1 depicts the variations of (a) $es_t$, (b) $ot$, (c) $tur$, and $cn$ with different heat loss coefficient ($h_{hl}$) when nine-years average meteorological data was used. In Fig. A1 (a), $es_t$ increased with the increase of $h_{hl}$. $es_t$ was $3.18\times10^5$ kWh and $3.68\times10^5$ kWh when $h_{hl}$ was 2 W/(m$^2$·K) and 12 W/(m$^2$·K), respectively. This meant that $es_t$ was increased by 15.8% when $h_{hl}$ varied from 2 W/(m$^2$·K) to 12 W/(m$^2$·K). In Fig. A1 (b), $ot$ increased with the increase of $h_{hl}$. $ot$ was € $3.18\times10^4$ and € $3.57\times10^4$ when $h_{hl}$ was 2 W/(m$^2$·K) and 12 W/(m$^2$·K), respectively. This meant that $ot$ was

increased by 12.2% when $h_{hl}$ varied from 2 W/(m$^2$·K) to 12 W/(m$^2$·K). In Fig. A1 (c), $tur$ was still 0 when $h_{hl}$ varied from 2 W/(m$^2$·K) to 12 W/(m$^2$·K). In Fig. A1 (d), $cn$ increased with the increase of $h_{hl}$. $cn$ was 240.3 tons and 278.3 tons when $h_{hl}$ was 2 W/(m$^2$·K) and 12 W/(m$^2$·K), respectively.

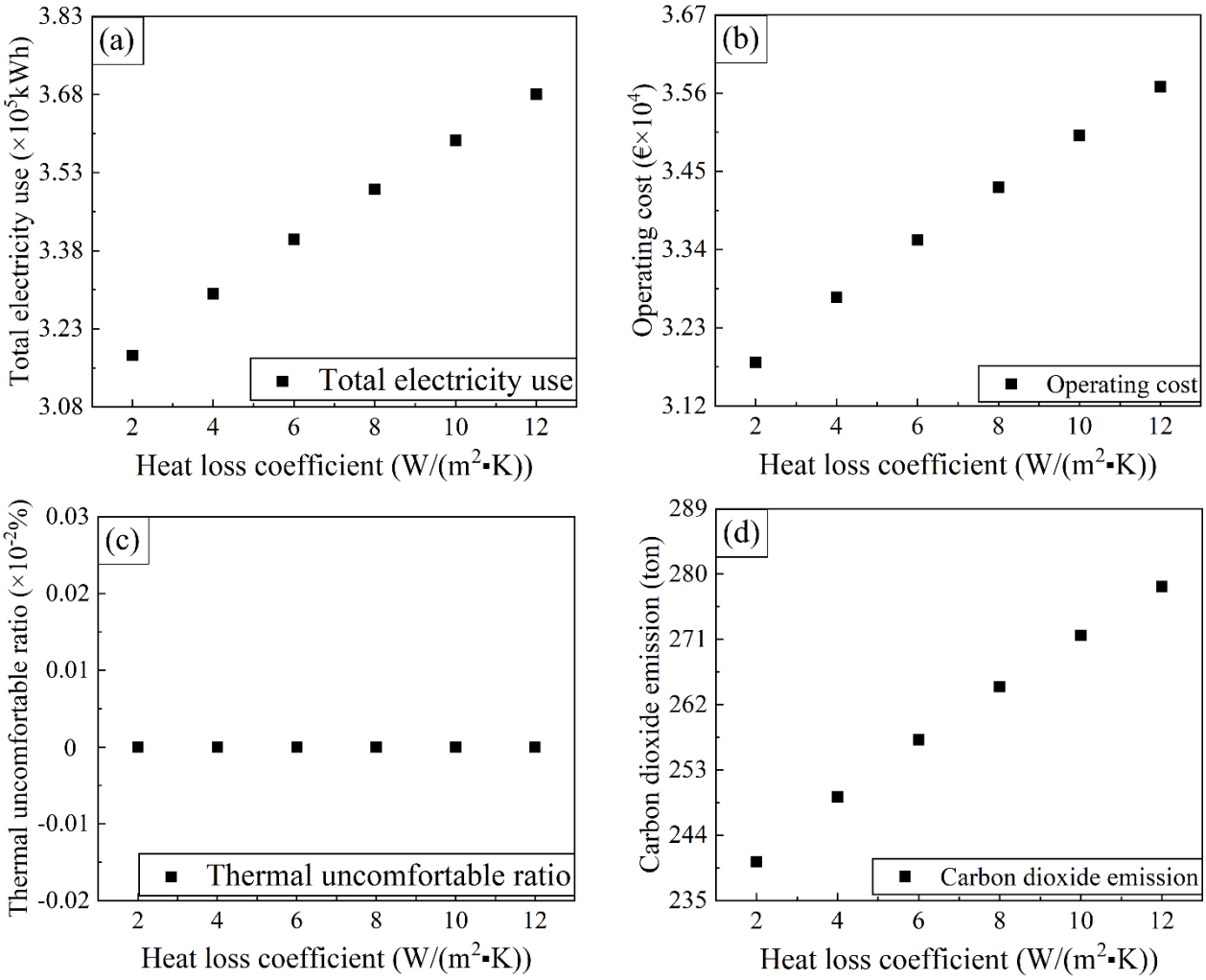


**Fig. A1** The variations of (a) total electricity use, (b) operating cost, (c) thermal uncomfortable ratio, and (d) $CO_2$ emission with different heat loss coefficients when nine-years average meteorological data was used

## Appendix B

The aim of the optimization was to maximize $S_o$ by identifying optimal $A_{SC}$ and $h_{hl}$, and thus the optimization problem could be expressed as Eqn. (B1):

$$(A_{SC}^*, h_{hl}^*) = \underset{A_{SC}, h_{hl}}{\operatorname{argmax}} S_o \tag{B1}$$

The maximum and minimum values of $A_{SC}$ were 5,500 m$^2$ and 2,000 m$^2$, respectively. The maximum and minimum values of $h_{hl}$ were 12 W/(m$^2$·K) and 2 W/(m$^2$·K), respectively. DESIGN EXPERT was applied to construct cubic models for $es_t$, $ot$, and $tur$. The cubic models could be expressed as Eqn. (B2):

$$U = h_0 + h_1 \cdot A_{SC,cx} + h_2 \cdot h_{hl,cx} + h_3 \cdot A_{SC,cx} \cdot h_{hl,cx} + h_4 \cdot A_{SC,cx}^2 + h_5 \cdot h_{hl,cx}^2 + h_6 \cdot A_{SC,cx}^2 \cdot h_{hl,cx} + h_7 \cdot h_{hl,cx}^2 \cdot A_{SC,cx} \quad \text{(B2)}$$

where $U$ denotes the response parameter. $h_0$, $h_1$, $h_2$, $h_3$, $h_4$, $h_5$, $h_6$, and $h_7$ are the coefficients for cubic model. $A_{SC,cx}$ and $h_{hl,cx}$ that are respectively the coded $A_{ST}$ and $h_{hl}$, are calculated by Eqns. (B3) and (B4):

$$A_{SC,cx} = \frac{2(A_{SC} - A_{SC,mn})}{A_{SC,mx} - A_{SC,mn}} - 1 \quad \text{(B3)}$$

$$h_{hl,cx} = \frac{2(h_{hl} - h_{hl,mn})}{h_{hl,mx} - h_{hl,mn}} - 1 \quad \text{(B4)}$$

where $mx$ and $mn$ denote the maximum and minimum values, respectively. Table B1 depicts the coefficients in cubic models for $es_t$, $ot$, and $tur$.

**Table B1** Coefficients in cubic models for $es_t$, $ot$, and $tur$

| | $es_t$ | $ot$ | $tur$ |
|---|---|---|---|
| $h_0$ | 3.40 | 3.36 | 0.6898 |
| $h_1$ | -0.1667 | -0.1287 | 0.1437 |
| $h_2$ | 0.2994 | 0.2312 | 0.3162 |
| $h_3$ | 0.0343 | 0.0265 | -0.0575 |
| $h_4$ | 0.0209 | 0.0162 | 0.3737 |
| $h_5$ | -0.0320 | -0.0246 | 0.0287 |
| $h_6$ | -0.0033 | -0.0026 | 0.0575 |
| $h_7$ | -0.0076 | -0.0059 | 0 |

In the case when $b_{ot}$, $b_{es_t}$, $b_{tur}$, and $b_{ct}$ were respectively 0.2, 0.2, 0.3, and 0.3, the maximum $S_o$ was 0.8, and the corresponding optimal $A_{SC}$ and $h_{hl}$ were 2,561.8 m$^2$ and 2 W/(m$^2$·K), respectively. In the case when $b_{ot}$, $b_{es_t}$, $b_{tur}$, and $b_{ct}$ were respectively 0.4, 0.3, 0.2, and 0.1, the maximum $S_o$ was 0.83, and the corresponding optimal $A_{SC}$ and $h_{hl}$ were 4,632.1 m$^2$ and 2 W/(m$^2$·K), respectively.

## Appendix C

Fig. C1 depicts the monthly average (a) dry bulb temperature, (b) wet bulb temperature, (c) wind speed and (d) solar irradiance. Note that the period for offering heat to the swimming pool was a winter season, i.e., from December 1st to April 30th. Thus, the weather data of December, January, February, March, and April were applied in this section. The maximum monthly average dry bulb temperature, wet bulb temperature, wind speed, and solar irradiance were 22.9°C, 21°C, 2.86 m/s, and 154 W/m$^2$, respectively. The minimum monthly average dry bulb temperature, wet bulb temperature, wind speed, and solar irradiance were 15.8°C, 13.3°C, 2.18 m/s, and 109 W/m$^2$, respectively.

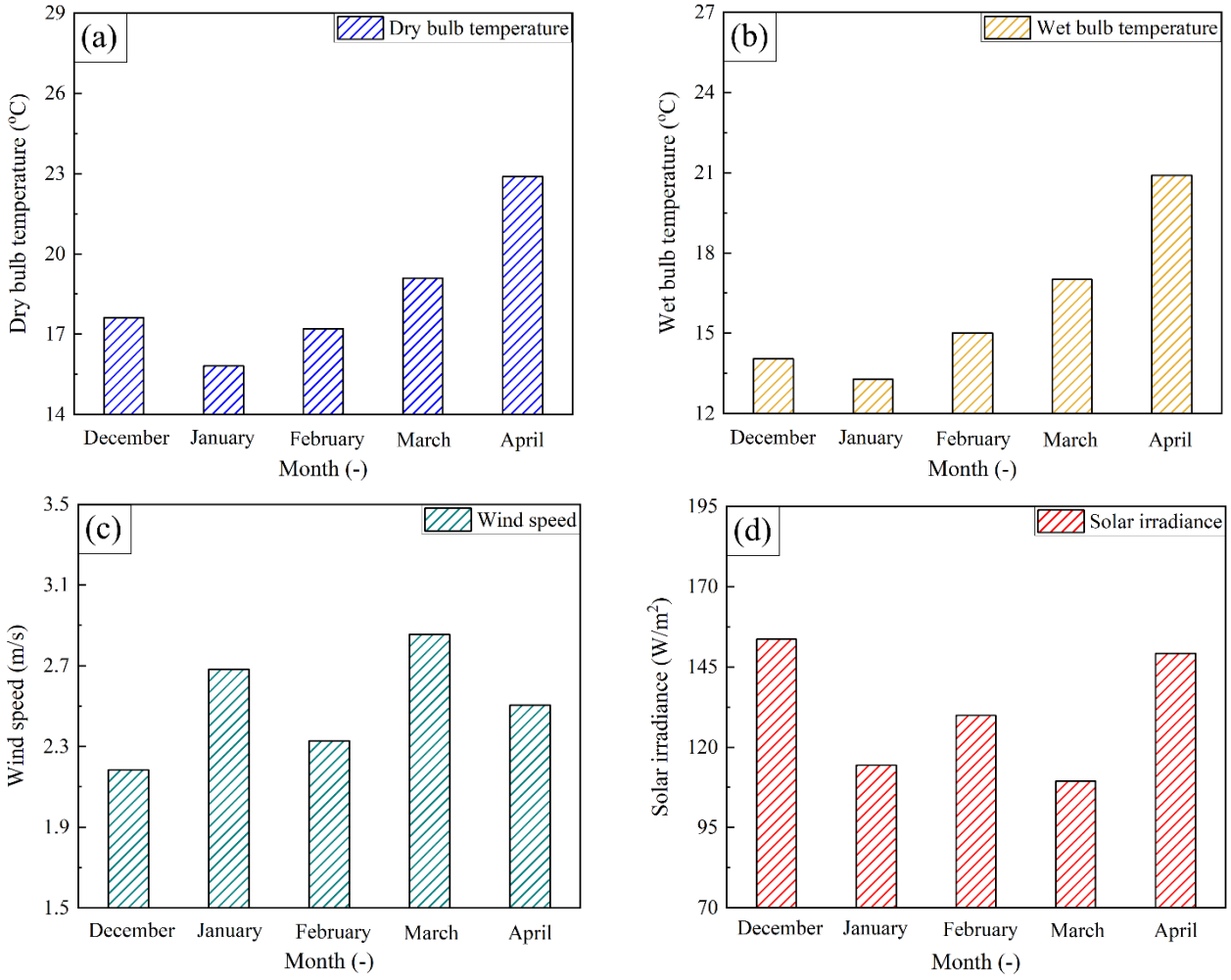


**Fig. C1.** The monthly average (a) dry bulb temperature, (b) wet bulb temperature, (c) wind speed and (d) solar irradiance

Fig. C2 depicts the variations of (a) $es_t$, (b) $ot$, (c) $tur$, and $cn$ in different months. In all the months, i.e., from December to April, $es_t$, $ot$, and $cn$ of the system with heat loss from PST were higher than those without heat loss from PST. The maximum $es_t$, $ot$, and $cn$ of the system with heat loss from PST were $7.64\times10^4$ kWh, €$1.28\times10^4$, and 57.8 ton, occurring at January, December, and January, respectively. The minimum $es_t$, $ot$, and $cn$ of the system with heat loss from PST were $5.79\times10^4$ kWh, €$4.48\times10^3$, and 43.8 ton. All these cases occurred at April. The maximum $es_t$, $ot$, and $cn$ of the system without heat loss from PST were $7.18\times10^4$ kWh, €$1.23\times10^4$, and 54.3 ton, occurring at January, December, and January, respectively. The minimum $es_t$, $ot$, and $cn$ of the system without heat loss from PST were $4.94\times10^4$ kWh, €$3.81\times10^3$, and 37.3 ton. All these cases occurred at April. $tur$ of the systems with and without heat loss from PST were still 0 in different months.

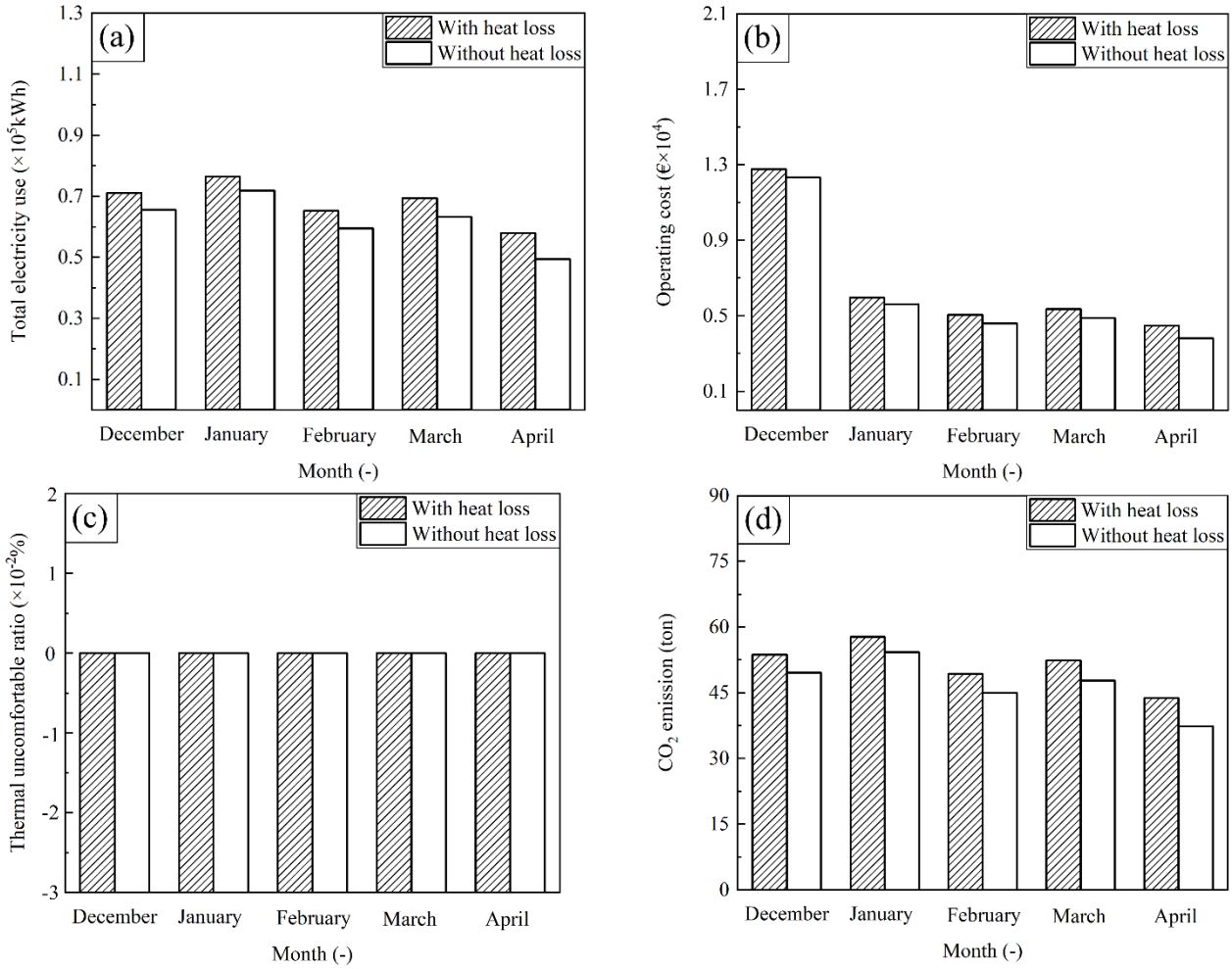


**Fig. C2.** (a) Total electricity use, (b) operating cost, (c) thermal uncomfortable ratio, and (d) $CO_2$ emission in different months

## Appendix D

Fig. D1 depicts the weekly average (a) dry bulb temperature, (b) wet bulb temperature, (c) wind speed, and (d) solar irradiance. The maximum weekly average dry bulb temperature, wet bulb temperature, wind speed, and solar irradiance were 21.8°C, 19.9°C, 2.96 m/s, and 168 W/m$^2$, respectively. The minimum weekly average dry bulb temperature, wet bulb temperature, wind speed, and solar irradiance were 9.3°C, 6.9°C, 1.14 m/s, and 20 W/m$^2$, respectively.

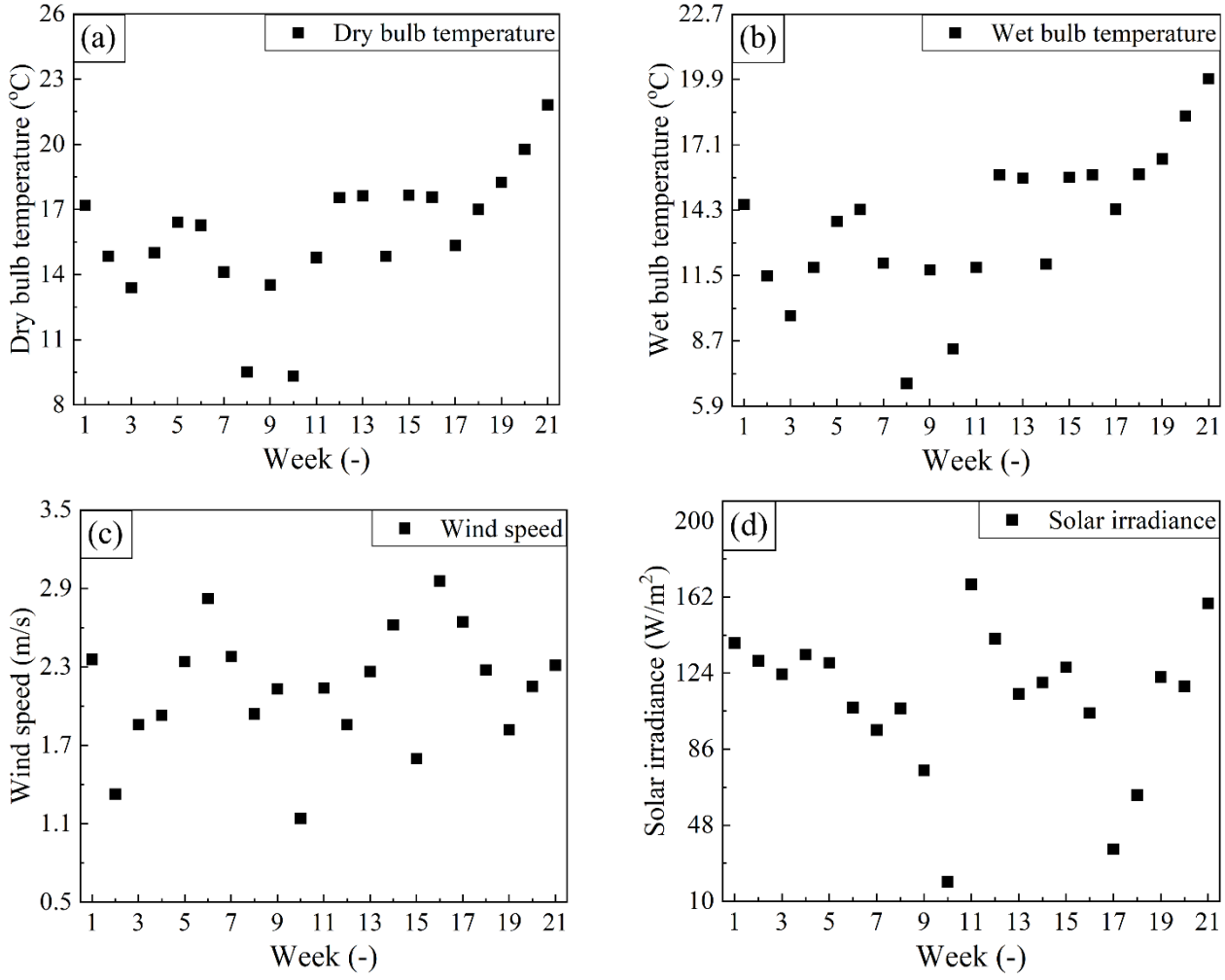


**Fig. D1.** The weekly average (a) dry bulb temperature, (b) wet bulb temperature, (c) wind speed and (d) solar irradiance

Fig. D2 depicts the variations of (a) $es_t$, (b) $ot$, (c) $tur$, and $cn$ in different months. In all the months, i.e., from the 1st week to 21st week, $es_t$, $ot$, and $cn$ of the system with heat loss from PST were higher than those without heat loss from PST. The maximum $es_t$, $ot$, and $cn$ of the system

with heat loss from PST were $1.84\times10^4$ kWh, €$8.52\times10^3$, and 13.9 ton, occurring at the 8th, 1st, and 8th weeks, respectively. Note that $ot$ for the 1st week was much larger than $ot$ for other weeks. Thus, $ot$ for the 1st week was not presented for better visual impression. The minimum $es_t$, $ot$, and $cn$ of the system with heat loss from PST were $1.22\times10^4$ kWh, €$9.38\times10^2$, and 9.2 ton. All these cases occurred at the 21st week. The maximum $es_t$, $ot$, and $cn$ of the system without heat loss from PST were $1.74\times10^4$ kWh, €$8.43\times10^3$, and 13.2 ton, occurring at the 8th, 1st, and 8th weeks. The minimum $es_t$, $ot$, and $cn$ of the system without heat loss from PST were $9.92\times10^3$ kWh, €$7.65\times10^2$, and 7.5 ton. All these cases occurred at the 21st week. $tur$ of the systems with and without heat loss from PST were still 0 in different weeks.

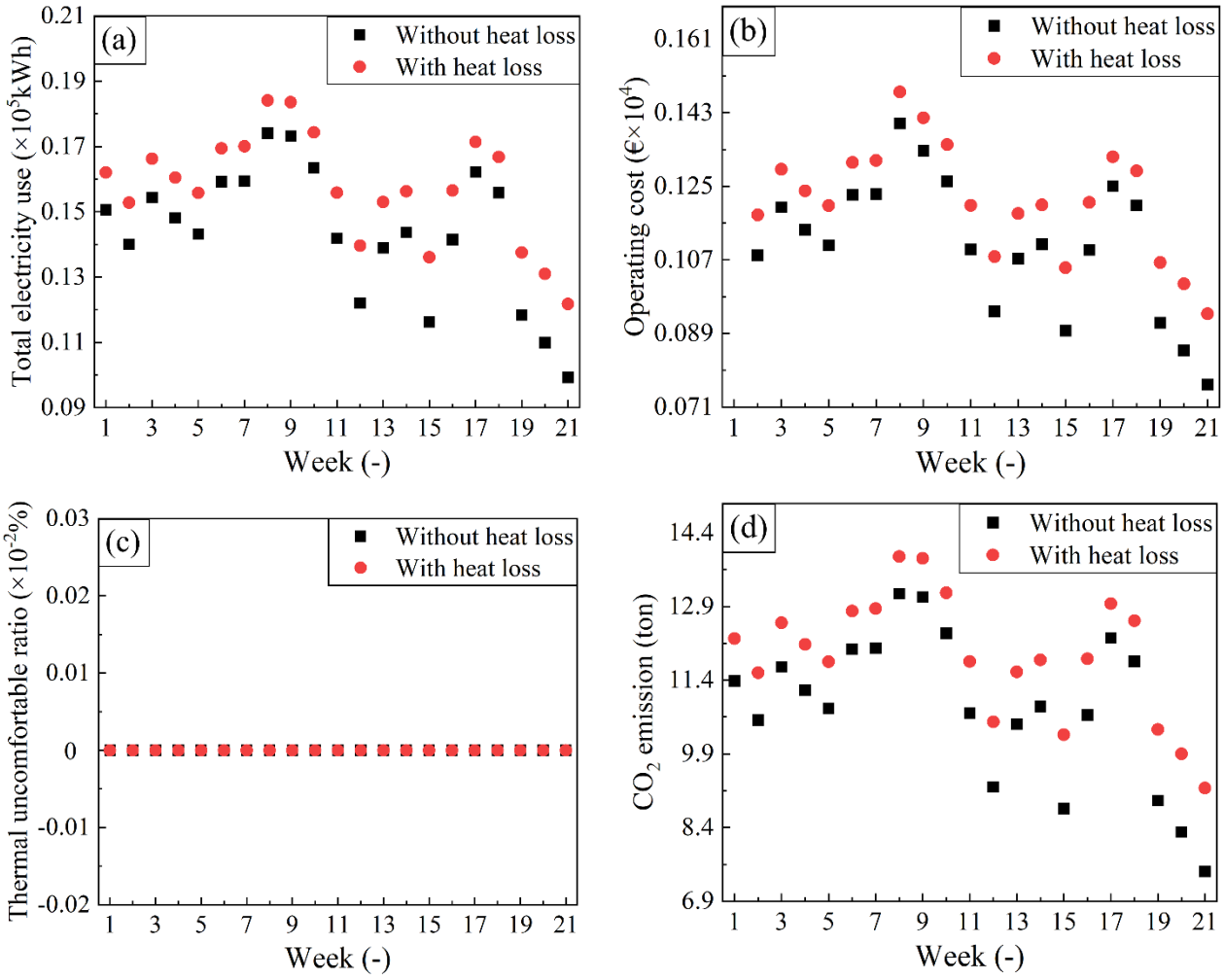


**Fig. D2.** (a) Total electricity use, (b) operating cost, (c) thermal uncomfortable ratio, and (d) $CO_2$ emission in different weeks

## References

[1] F.C. De La Torre, M. Varo, R. López-Luque, J. Ramírez-Faz, L. Fernández-Ahumada, Design and analysis of a tracking/backtracking strategy for PV plants with horizontal trackers after their conversion to agrivoltaic plants, Renewable Energy 187 (2022) 537-550. https://doi.org/10.1016/j.renene.2022.01.081

[2] Y. Li, N. Nord, H. Wu, Z. Yu, G. Huang, A study on the integration of air-source heat pumps, solar collectors, and PCM tanks for outdoor swimming pools for winter application in subtropical climates, Journal of Building Performance Simulation 13(6) (2020) 662-683. https://doi.org/10.1080/19401493.2020.1813198

[3] A. Arabgolarcheh, D. Micallef, A. Rezaeiha, E. Benini, Modelling of two tandem floating offshore wind turbines using an actuator line model, Renewable Energy 216 (2023) 119067. https://doi.org/10.1016/j.renene.2023.119067

[4] S.A.A. Naqvi, M. Hussain, B. Hussain, S.A.R. Shah, J. Nazir, M. Usman, Environmental sustainability and biomass energy consumption through the lens of pollution Haven hypothesis and renewable energy-environmental kuznets curve, Renewable Energy 212 (2023) 621-631. https://doi.org/10.1016/j.renene.2023.04.127

[5] M. Nasir, A.R. Jordehi, S.A.A. Matin, V.S. Tabar, M. Tostado-Véliz, S.A. Mansouri, Optimal operation of energy hubs including parking lots for hydrogen vehicles and responsive demands, Journal of Energy Storage 50 (2022) 104630. https://doi.org/10.1016/j.est.2022.104630

[6] A. de Fockert, A.C. Bijlsma, T.S. O'Mahoney, W. Verbruggen, P.C. Scheijgrond, Z.B. Wang, Assessment of the impact of tidal power extraction from the Eastern Scheldt storm surge barrier through the evaluation of a pilot plant, Renewable Energy (2023) 109-120. https://doi.org/10.1016/j.renene.2023.06.001

[7] T. You, F. Wang, Green ground source heat pump using various low-global-warming-potential refrigerants: Thermal imbalance and long-term performance, Renewable Energy 210 (2023) 159-173.http://dx.doi.org/10.1016/j.renene.2023.04.058

[8] Y. Li, N. Nord, N. Zhang, C. Zhou, An ANN-based optimization approach of building energy systems: Case study of swimming pool, Journal of Cleaner Production 277 (2020) 124029.http://dx.doi.org/10.1016/j.jclepro.2020.124029

[9] Y. Li, N. Nord, H. Yin, An investigation of using $CO_2$ heat pumps to charge PCM storage tank for domestic use, Renewable Energy (2023) 119279.http://dx.doi.org/10.1016/j.renene.2023.119279
[10] S. Thorsteinsson, A.A.S. Kalaee, P. Vogler-Finck, H.L. Stærmose, I. Katic, J.D. Bendtsen, Long-term experimental study of price responsive predictive control in a real occupied single-family house with heat pump, Applied Energy 347 (2023) 121398.http://dx.doi.org/10.1016/j.apenergy.2023.121398
[11] X. Hao, Y. Zhou, Q. Wang, N. Gao, X. Wang, G. Chen, Prospective study of a novel heat pump system with solar energy spectral beam splitting, Renewable Energy 217 (2023) 119209.http://dx.doi.org/10.1016/j.renene.2023.119209
[12] W. Chen, X. Li, T. Li, W. Shi, B. Wang, Y. Cao, Design method of general heat exchanger networks with heat pumps based on thermal energy discretization and matching, Journal of Cleaner Production 384 (2023) 135620.http://dx.doi.org/10.1016/j.jclepro.2022.135620
[13] A.J. Pimm, T.T. Cockerill, W.F. Gale, Reducing industrial hydrogen demand through preheating with very high temperature heat pumps, Applied Energy 347 (2023) 121464.http://dx.doi.org/10.1016/j.apenergy.2023.121464
[14] S. Lee, Y. Chung, S. Kim, Y. Jeong, M.S. Kim, Predictive optimization method for the waste heat recovery strategy in an electric vehicle heat pump system, Applied Energy 333 (2023) 120572. https://doi.org/10.1016/j.apenergy.2022.120572
[15] J.T. Gao, Z.Y. Xu, R.Z. Wang, An air-source hybrid absorption-compression heat pump with large temperature lift, Applied Energy 291 (2021) 116810.http://dx.doi.org/10.1016/j.apenergy.2021.116810
[16] K. Sezen, A. Gungor, Comparison of solar assisted heat pump systems for heating residences: A review, Solar Energy 249 (2023) 424-445.http://dx.doi.org/10.1016/j.solener.2022.11.051
[17] X. Yu, Z. Guo, Z. Gao, B. Yang, X. Ma, S. Dong, Thermodynamic investigation of a direct-expansion solar assisted heat pump with evacuated tube collector-evaporator, Renewable Energy 206 (2023) 418-427.http://dx.doi.org/10.1016/j.renene.2023.01.112
[18] T. Zhang, Y.F. Zhang, Z.R. Shi, Q.F. Li, J.Y. Cai, Experimental study of a photovoltaic solar-assisted heat pump/gravity-assisted heat pipe hybrid system, Renewable Energy 207 (2023) 147-161.http://dx.doi.org/10.1016/j.renene.2023.03.008

[19] X. Gu, J. Dai, H. Li, Y. Dai, Experimental and theoretical assessment of a solar assisted heat pump system for in-bin grain drying: A comprehensive case study, Renewable Energy 181 (2022) 426-444.http://dx.doi.org/10.1016/j.renene.2021.09.049
[20] Z. Song, J. Ji, J. Cai, B. Zhao, Z. Li, Investigation on a direct-expansion solar-assisted heat pump with a novel hybrid compound parabolic concentrator/photovoltaic/fin evaporator, Applied Energy 299 (2021) 117279.http://dx.doi.org/10.1016/j.apenergy.2021.117279
[21] Y. Wang, Z. Quan, Y. Zhao, L. Wang, Z. Liu, Performance and optimization of a novel solar-air source heat pump building energy supply system with energy storage, Applied Energy 324 (2022) 119706.http://dx.doi.org/10.1016/j.apenergy.2022.119706
[22] T.T. Chow, Y. Bai, K.F. Fong, Z. Lin, Analysis of a solar assisted heat pump system for indoor swimming pool water and space heating, Applied Energy 100 (2012) 309-317.http://dx.doi.org/10.1016/j.apenergy.2012.05.058
[23] Y. Li, G. Huang, T. Xu, X. Liu, H. Wu, Optimal design of PCM thermal storage tank and its application for winter available open-air swimming pool, Applied Energy 209 (2018) 224-235.http://dx.doi.org/10.1016/j.apenergy.2017.10.095
[24] S. Rahmanian, H. Rahmanian-Koushkaki, M. Moein-Jahromi, R. Saidur, A novel method to improve the performance of PCM thermal energy storage units using a small oscillator plate-numerical analysis, Journal of Energy Storage 73 (2023) 108900.http://dx.doi.org/10.1016/j.est.2023.108900
[25] H.-O. Sayehvand, S. Abolfathi, B. Keshavarzian, Investigating heat transfer enhancement for PCM melting in a novel multi-tube heat exchanger with external fins, Journal of Energy Storage 72 (2023) 108702.http://dx.doi.org/10.1016/j.est.2023.108702
[26] D.-X. Zhang, C.-Y. Zhu, X.-Y. Duan, L. Gong, B.-H. Huang, M.-H. Xu, Y. Chen, Design and transient temperature control performance analysis of a novel hybrid PCM-based heat sink, Journal of Energy Storage 72 (2023) 108450.http://dx.doi.org/10.1016/j.est.2023.108450
[27] W. Kong, G. Wang, G. Englmair, E.N.N. Nielsen, J. Dragsted, S. Furbo, J. Fan, A simplified numerical model of PCM water energy storage, Journal of Energy Storage 55 (2022) 105425.http://dx.doi.org/10.1016/j.est.2022.105425
[28] Y. Li, Z. Niu, X. Gao, R. Ji, X. Yang, J. Yan, Experimental and numerical investigations on tilt filling design of metal foam in a heat storage tank, Renewable Energy 217 (2023) 119167.http://dx.doi.org/10.1016/j.renene.2023.119167

[29] Z.N. Meng, P. Zhang, Experimental and numerical investigation of a tube-in-tank latent thermal energy storage unit using composite PCM, Applied Energy 190 (2017) 524-539.http://dx.doi.org/10.1016/j.apenergy.2016.12.163

[30] H. Liang, L. Liu, Z. Zhong, Y. Gan, J.-Y. Wu, J. Niu, Towards idealized thermal stratification in a novel phase change emulsion storage tank, Applied Energy 310 (2022) 118526.http://dx.doi.org/10.1016/j.apenergy.2022.118526

[31] Y. Li, G. Huang, H. Wu, T. Xu, Feasibility study of a PCM storage tank integrated heating system for outdoor swimming pools during the winter season, Applied Thermal Engineering 134 (2018) 490-500.http://dx.doi.org/10.1016/j.applthermaleng.2018.02.030

[32] Heat loss coefficient, 2023. http://www.conserveandsave.co.uk/calculations/heat-loss

[33] Hong Kong Observatory, 2024. https://www.hko.gov.hk/en/index.html.

[34] A.A. Bawazir, D. Friedrich, Evaluation and design of large-scale solar adsorption cooling systems based on energetic, economic and environmental performance, Energies 15(6) (2022) 2149.https://doi.org/10.3390/en15062149

[35] A. Lisauskas, Solar calculations for the Raseiniai district heating plant, Laboratory of regional energy developement, Lithuanian energy institute, 2014.

[36] A.P. Melo, R. Lamberts, Envelope insulation and heat balance in commercial buildings, (2009).

[37] J. Ye, K. Yang, H. Ye, A. Emadi, A Fast Electro-Thermal Model of Traction Inverters for Electrified Vehicles, IEEE Transactions on Power Electronics 32(5) (2017) 3920-3934.http://dx.doi.org/10.1109/tpel.2016.2585526